Melt-rock interaction in the lower crust based on silicate melt inclusions in mafic garnet granulite xenoliths, Bakony–Balaton Highland Volcanic Field (Hungary)

BIANKA NÉMETH[1,2,3,✉], KÁLMÁN TÖRÖK[1], ENIKŐ BALI[4], ZOLTÁN ZAJACZ[5], LÁSZLÓ FODOR[6,7] and CSABA SZABÓ[3]

[1]Mining and Geological Survey of Hungary, Stefánia Road 14., Budapest, H-1143, Hungary;
✉nemethbj@student.elte.hu, torok.kalman@mbfsz.gov.hu
[2]MTA-ELTE Volcanology Research Group, Eötvös University, Pázmány Péter sétány 1/c, Budapest, H-1117, Hungary
[3]Lithosphere Fluid Research Lab (LRG), Department of Petrology and Geochemistry, Eötvös Loránd University, Pázmány Péter sétány 1/c, Budapest, H-1117, Hungary; csaba.szabo@ttk.elte.hu
[4]Nordic Volcanological Institute, Institute of Earth Sciences, University of Iceland, Sturlugata 7, 101 Reykjavík, Iceland; eniko@hi.is
[5]Department of Earth Sciences, Institute of Isotope Geochemistry and Mineral Resources, ETH Zürich, 8092 Zürich, Switzerland; present day address: Section of Earth and Environmental Sciences, University of Geneva, Switzerland; zoltan.zajacz@unige.ch
[6]Department of Geology, Eötvös Loránd University, Pázmány Péter sétány 1/c, Budapest, H-1117, Hungary; imre.laszlo.fodor@ttk.elte.hu
[7]MTA-ELTE Geological, Geophysical and Space Science Research Group, Eötvös University, Pázmány Péter sétány 1/c, Budapest, H-1117, Hungary

Abstract: Major and trace element composition of silicate melt inclusions (SMI) and their rock-forming minerals were studied in mafic garnet granulite xenoliths from the Bakony–Balaton Highland Volcanic Field (Western Hungary). Primary SMIs occur in clinopyroxene and plagioclase in the plagioclase-rich domains of mafic garnet granulites and in ilmenite in the vicinity of these domains in the wall rock. Based on major and trace elements, we demonstrated that the SMIs have no connection with the xenolith-hosting alkaline basalt as they have rhyodacitic composition with a distinct REE pattern, negative Sr anomaly, and HFSE depletion. The trace element characteristics suggest that the clinopyroxene hosted SMIs are the closest representation of the original melt percolated in the lower crust. In contrast, the plagioclase and ilmenite hosted SMIs are products of interaction between the silicic melt and the wall rock garnet granulite. A further product of this interaction is the clinopyroxene–ilmenite±plagioclase symplectite. Textural observations and mass balance calculations reveal that the reaction between titanite and the silicate melt led to the formation of these assemblages. We propose that a tectonic mélange of metapelites and (MOR-related) metabasalts partially melted at 0.3–0.5 GPa to form a dacitic–rhyodacitic melt leaving behind a garnet-free, plagioclase+clinopyroxene+orthopyroxene+ilmenite residuum. The composition of the SMIs (both major and trace elements) is similar to those from the middle Miocene calc-alkaline magmas, widely known from the northern Pannonian Basin (Börzsöny and Visegrád Mts., Cserhát and Mátra volcanic areas and Central Slovakian VF), but the SMIs are probably the result of a later, local process. The study of these SMIs also highlights how crustal contamination changes magma compositions during asthenospheric Miocene ascent.

Keywords: partial melting, crustal contamination, anatexis, peraluminous granitoid melt, silicate melt inclusion, mafic granulite, trace elements.

Introduction

The continental crust melts under different pressure (p) and temperature (T) conditions depending on the rock composition (X) and the presence of H_2O. Migration of granitic anatectic magmas is the main process of crustal differentiation which leaving behind restitic granulites as residual, garnet- and pyroxene-rich complements of these magmas, devoid of amphibole or biotite (Clemens 1990).

Since water plays a fundamental role in decreasing the melting temperature of rocks, any form of it has a significant impact on melting. Crustal melting can be a water-fluxed process in the presence of a free H_2O phase or alternatively can be a fluid-absent melting. In the presence of aqueous fluids, the generated melt can be water-rich or water-saturated.

In the absence of an aqueous fluid, the break-down of hydrous minerals such as muscovite or biotite controls melting in metapelites or amphibole in metabasic rocks in order of increasing temperature. These latter processes are called dehydration melting reactions, where all water is derived from hydrous minerals and the generated melt is water-undersaturated (e.g., Weinberg & Hasalová 2015, and references therein).

Dehydration melting can be accompanied by infiltration of low H_2O-activity fluids, which can be hypersaline or rich in CO_2 or both (Peterson & Newton 1990; Manning & Aranovich 2014; Aranovich 2017; Manning 2018). These fluids are characteristic of the lower crust and the lithospheric mantle (e.g., Touret 1985; Newton et al. 1998). The chemistry of the produced melt changes from granodioritic to tonalitic, depending on the pressure and temperature conditions of the melting,

the original mineral assemblage and the rate of the partial melting and (e.g., Castro et al. 1999; Qian & Hermann 2013). Where metamorphism is accompanied by magmatism, as in volcanic arcs, the crystallization of magmas in the deep crust leads to the input of externally derived magmatic fluids into deep-crustal metamorphic systems (e.g., Annen et al. 2005).

Fluid and melt inclusions have been extensively used in igneous petrology because they can preserve chemical and physical information of the original magmatic system (e.g., Roedder 1992; Frezzotti 2001; Bodnar & Frezzotti 2020). In high-grade metamorphic rocks, the presence of fluid inclusions is widely known (e.g., Touret & Huizenga 2020), but melt inclusions are less common (Cesare et al. 2015; Bartoli et al. 2016; Bartoli & Cesare 2020). Anatectic melt composition derived from various parental rocks are generally estimated based on the composition in magmatic leucosomes (e.g. Sawyer 1987) and from experimental works (e.g., Vielzeuf & Schmidt 2001). Leucosomes, however, might be modified by fractional crystallization or segregation processes, whereas experimental works rarely reproduce natural compositions at low degrees of partial melting.

The aim of this research is to study granulite xenoliths in which melt migration can be observed in the form of melt pockets and associated silicate melt inclusions. The location of the studied mafic garnet granulite xenoliths is the Bakony–Balaton Highland Volcanic Field (BBHVF), from the western Pannonian Basin. Although silicate melt inclusions are widely studied in mantle rocks in the Pannonian Basin (e.g., Török et al. 2003; Bali et al. 2007; Zajacz et al. 2007; Hidas et al. 2010; Créon et al. 2017), no report has been published on silicate melt inclusions of crustal origin.

In the last few years, research on silicate melt inclusions in high-grade metamorphic rocks has come to focus (e.g., Nicoli & Ferrero 2021, and references therein). However, these studies show, that most of these inclusions are trapped in rocks with sedimentary protoliths and that such inclusions are partially or completely crystallized and therefore called nanogranites. These nanogranites are now widely known in felsic granulites and are attributed to crustal anatexis (e.g., Cesare et al. 2009, 2011, 2015; Ferrero et al. 2012, 2015; Barich et al. 2014; Hiroi et al. 2019, 2020; Tacchetto et al. 2019; Bartoli & Cesare 2020). These primary silicate melt inclusions are thought to be trapped in peritectic minerals formed by incongruent melting reactions.

In this paper, glassy (glass+bubble) silicate melt inclusions were studied from mafic granulites. Primary silicate melt inclusions exist in the rock-forming minerals of the studied xenoliths, which provide melt composition and direct evidence of partial melting processes, as well as melt/fluid-rock interactions in the deep crust.

Highly refractory granulite xenoliths have been described from the BBHVF's lower crust (Török 1995, 2012; Dobosi et al. 2003; Embey-Isztin et al. 2003; Török et al. 2005; Dégi et al. 2009, 2010) indicating an earlier partial melting process. Besides, some migmatite-like xenoliths with garnet–clinopyroxene–orthopyroxene–plagioclase melanosome and plagio-clase+clinopyroxene±orthopyroxene leucosome were also discovered.

Fluid inclusions and mineral chemistry of the xenoliths in question were studied by Németh et al. (2015). They presented direct evidence for melt/fluid-rock interaction, such as melt inclusion-bearing, garnet-free, plagioclase–clinopyroxene veins and patches in the garnet granulites, clinopyroxene–ilmenite±plagioclase symplectites with titanite relics and embayed symplectites after garnets in the wall rock, next to the vein and patches. FTIR spectroscopic data showed that minerals in the plagioclase-rich domains were richer in structural hydroxyl groups than those in the host mafic garnet granulite, indicating partial rehydration of the highly dehydrated mafic garnet granulite by fluids and melts (Németh et al. 2015). The minerals show chemically different compositions according to their petrographic positions (Németh et al. 2015). However, the composition and origin of the silicate melt metasomatizing the refractory garnet granulite remained uncertain. In this study, we address these questions using major and trace element analyses of melt inclusions and their host minerals as well as of the inclusion-free minerals in two garnet granulite xenoliths.

Geological setting

The Miocene to Quaternary Pannonian Basin (central Europe) is superimposed on the Alpine–Carpathian–Dinaridic orogen, which formed during long-lasting contractional deformation started in the late Jurassic (Schmid et al. 2008). The pre-rift formations of the Pannonian Basin (PB) are built up by the ALCAPA (ALpine–CArpathian PAnnonian) and the Tisza–Dacia units juxtaposed along the Mid-Hungarian Zone (MHZ) (Csontos et al. 1992; Fig. 1a). The northern ALCAPA block was extruded from the Alps (Kázmér & Kovács 1985; Schmid et al. 2008) and it presumably had similarly thickened crust that of the Eastern Alps. The driving force of this process was the post-collisional shortening between the stable European and the Adriatic plates (Csontos & Vörös 2004). During the extrusion, the ALCAPA unit displaced eastward as a crustal flake or a single lithospheric unit during the late Oligocene–early Miocene (Fodor et al. 1999; Kovács & Szabó 2008; Horváth et al. 2015) meanwhile Adria moved northward. This event was followed by the early to middle Miocene extensional phase of the Pannonian Basin partly caused by subduction processes beneath the Carpathians and the Dinarides (Royden 1988; Maţenco & Radivojević 2012). This syn-rift extension was accompanied by intensive calc-alkaline volcanism (e.g., Szabó et al. 1992; Harangi & Lenkey 2007). The syn-rift extension migrated in space and terminated only in the early late Miocene (up to ~9 Ma) in the basin centre (Balázs et al. 2016) while modest extension was still active up to 8.7 Ma in the study area (Fodor et al. 2021). The extension could be associated with an asthenosphere upwelling (Horváth 1993) followed by OIB type alkaline basaltic magmatism (Embey-Isztin et al. 1993).
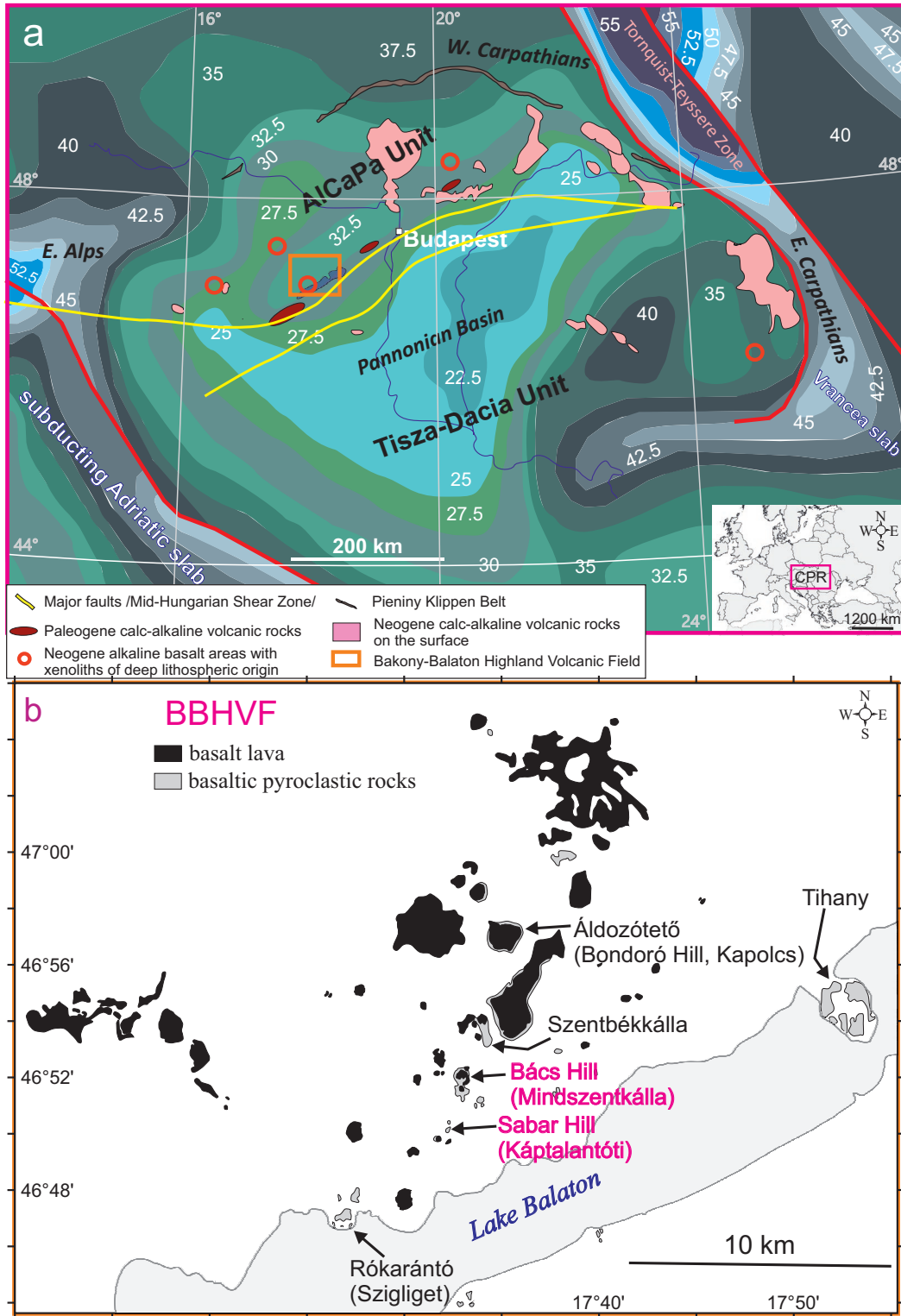
Fig. 1. Schematic map of the studied area with the present-day crustal thickness and the locations of the lower crustal granulite xenoliths. **a** — Schematic map of the present-day crustal thickness of the Carpathian–Pannonian Region modified after Horváth et al. (2015) with the main tectonic units (ALCAPA and Tisza–Dacia). The red lines refer to major changes in lithospheric thickness. Note that the thickness of the crust is growing towards the Alps. The colour of the different crust-thickness regions become darker with thickness, starting in green then following in grey and finishing in blue. The white numbers mark the thickness in km. **b** — Schematic map of the Bakony–Balaton Highland Volcanic Field with the locations of the lower crustal xenoliths hosted by basaltic lava and pyroclast modified after Jugovics (1968) and Harangi (2001). The two highlighted locations, Sabar Hill and Bács Hill show the location of the studied granulite xenoliths. The brackets hide the closest village names to the locations. The mark on both side of the map frame is the square grid from the original map to help mark the map as accurately as possible.

There are five alkaline basaltic volcanic fields (VF) known on the surface within the CPR where the xenoliths from the deep lithosphere were transported to the surface (Fig. 1a). These are the Styrian Basin VF, the Little Hungarian Plain VF, the Bakony–Balaton Highland VF (BBHVF), the Nógrád–Gömör VF, and the Perşani Mountains VF. In the study area, the BBHVF, this alkaline basaltic volcanism occurred between 7.9 and 2.8 Ma ago (Balogh et al. 1994; Wijbrans et al. 2007).

The BBHVF is located in the western-central PB, on the ALCAPA unit (Fig. 1a and b). This volcanic area is the richest in lower crustal xenoliths within the CPR. Six xenolith bearing locations are known in the BBHVF. These are Rókarántó (Szigliget village), Tihany, Áldozótető (Bondoró Hill, close to Kapolcs village), Szentbékkálla, Bács Hill (46°51'57.2"N, 17°31'41.0"E; near Mindszentkálla village), and Sabar Hill (46°51'03.3"N, 17°31'44.9"E; near Káptalantóti village), (Fig. 1b). The xenoliths can be found scattered throughout the local vineyards.

The dominant lower crustal xenoliths are garnet-bearing mafic granulites (Török 1995; Kempton et al. 1997; Dégi & Török 2003; Dobosi et al. 2003; Embey-Isztin et al. 2003; Török et al. 2005; Dégi et al. 2009, 2010), but there are metasedimentary ones as well (Embey-Isztin et al. 2003; Downes et al. 2015). Other types of granulites, include clinopyroxene–plagioclase felses, buchites (ultrahigh temperature, low pressure metamorphic rocks), and some felsic granulites from the middle crust (e.g., Török 2002, 2012; Török et al. 2014), whereas fragments of the upper crust also occur (Török et al. 2005; Török 2012). Two types of mafic granulite were observed and distinguished based on their mineral assemblages. The "dry" granulites are composed of clinopyroxene+garnet+plagioclase±orthopyroxene±quartz±scapolite±oxides. The "wet" granulites contain additional OH-bearing minerals such as amphibole or biotite. A continuous lithostratigraphic lower crustal profile was proposed by these workers with a paleo-depth range from 35 to 58 km, which indicates a thicker, paleo-lower crust than the present-day one beneath the Pannonian Basin (25–32 km; Posgay et al. 1991; Kalmár et al. 2018) and shows values similar to the present-day thickness of the crust beneath the Alps (50–56 km; Török 2012).

Analytical techniques

The major element composition of the minerals and SMIs were measured by Cameca SX-100 type electron microprobe equipped with wavelength-dispersive spectrometers at the Institute of Earth Sciences, Vienna University. The accelerating voltage was 20 keV and the beam current was 20 nA. The electron beam diameter changed between 1–5 microns. ZAF correction was applied for the precise quantitative determination of elements. Some of the BSE images were also taken by an AMRAY 1830 I/T6 type scanning electron microscope equipped by EDAX PV 9800 energy-dispersive

spectrometer at the Institute of Earth Sciences, Eötvös University Budapest. The accelerating voltage and the beam current were the same as in Vienna.

Trace element composition of the minerals and the unheated SMIs were measured by Laser Ablation–Inductively Coupled Plasma Mass Spectrometry (LA–ICPMS) at ETH Zürich. The system consisted of a prototype ArF excimer UV (193 nm) laser ablation system (analogue to Geolas) coupled with an ELAN 6100 DRC quadrupole mass spectrometer. About 8 J/cm^2 energy density on the sample surface and a repetition rate of 10 Hz was used. The energy density was homogeneous across the laser beam profile (Heinrich et al. 2003). The beam diameter was adjusted between 20 to 80 µm to a slightly larger value than the actual size of the inclusions to avoid incomplete sampling of the SMIs. 10 ms dwell time was used for the elements. The external standard was Glass NIST SRM 610. Unheated SMIs (containing only glass±bubbles) were ablated with their host minerals (Halter et al. 2002). Quantification of the SMI analyses followed the method of Zajacz & Halter (2007). We used the average K$_2$O content of the melt inclusions, determined by EPMA, as an internal standard. The data processing was carried out by the data analyses software SILLS (Guillong et al. 2008). For the host minerals of the SMIs, the beam diameter was the same as for the inclusions. For inclusion-free minerals, the beam size was 40–70 µm and 100 % major element oxide total was used as internal standard (Halter et al. 2002; Heinrich et al. 2003).

Results

Petrography

Lower crustal garnet granulite xenoliths from the BBHVF can be divided into two major groups based on microscopic observations. One group is characterized by a microstructural equilibrium mineral association with 120° grain boundaries (e.g., Embey-Isztin et al. 1993; Török 1995; Kempton et al. 1997; Dobosi et al. 2003), whereas the other group contains xenoliths with different mineral reaction domains (e.g., symplectites and reaction coronas after garnet and titanite) and thus texturally non-equilibr. The latter xenoliths provide valuable information of crustal evolution in extensional environment. There are xenoliths with relics of OH-bearing minerals (biotite or amphibole, Fig. 2a) and there are some with metasomatic amphiboles. However, anhydrous minerals can also be affected during these reactions, such as breakdown of garnet, titanite or scapolite, moreover, in some cases, peritectic crystallization of garnet (Fig. 2b).

In this paper, we focused on two xenoliths which have SMIs.

Xenolith petrography

The basic petrographic observations in the two selected granulite samples (Sabar Hill-Sab28 and Mindszentkálla-Mi26)
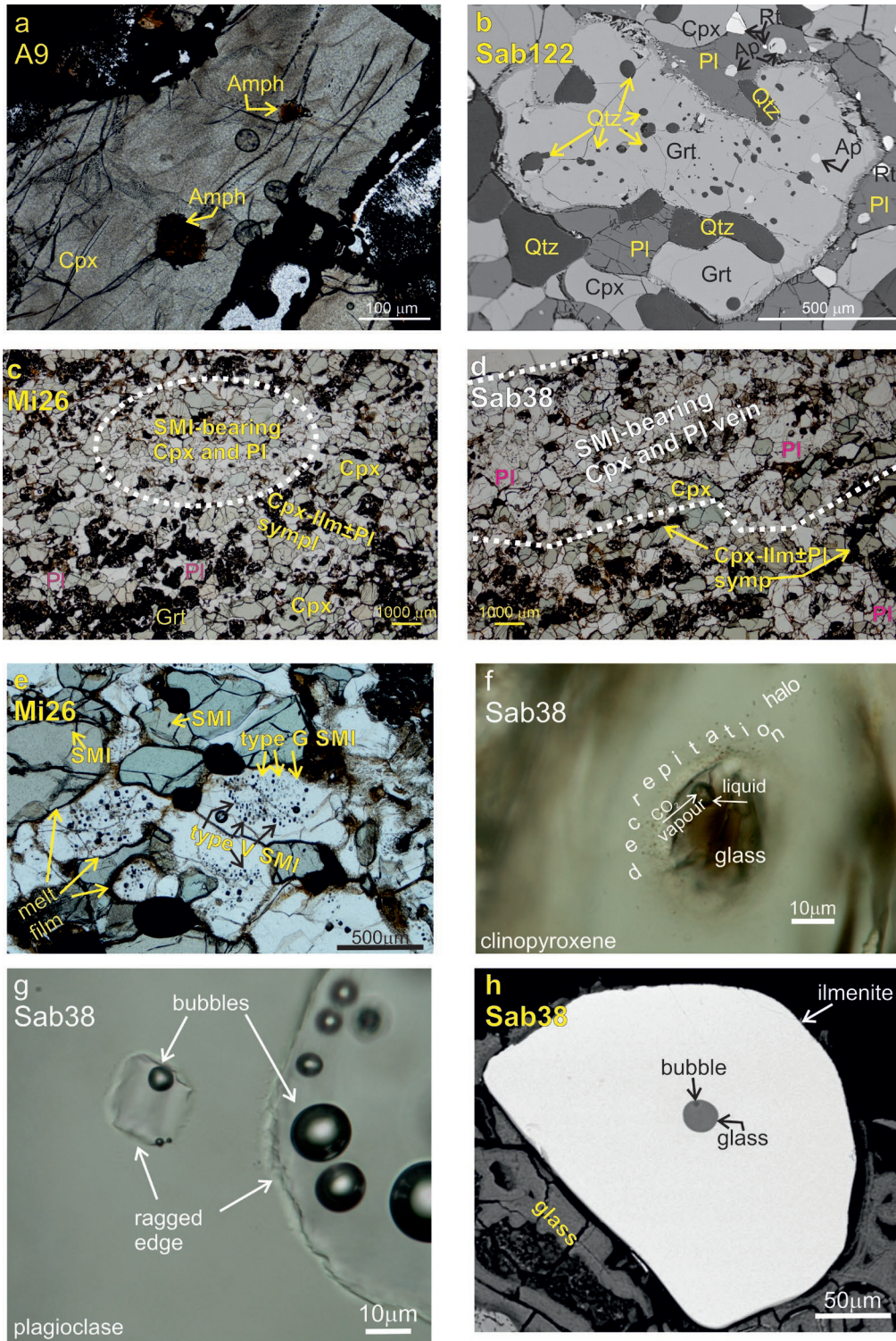
Fig. 2. Photomicrographs of the characteristic textural features in garnet granulite xenoliths. Mineral abbreviations follow Kretz (1983). **a** — Photomicrograph of amphibole inclusions in clinopyroxene from A9 granulite xenolith, from Áldozótető location. **b** — Backscattered electron image of peritectic garnet with quartz inclusions from Sab122 granulite xenolith. **c** — Photomicrograph of the silicate melt inclusion-bearing plagioclase–clinopyroxene mineral assemblage, and of the surrounding silicate melt inclusions-free minerals in Mi26 granulite xenolith. **d** — Photomicrograph of the silicate melt inclusion-bearing plagioclase–clinopyroxene vein at the edge of Sab38 granulite xenolith, with the adjacent wall rock with melt inclusion-free minerals. **e** — Photomicrograph of primary silicate melt inclusions in the rock-forming minerals, such as plagioclase and clinopyroxene in Mi26 granulite xenolith. Note that glassy (type G) and vapour dominated (type V) silicate melt inclusions are together in plagioclase host minerals. **f** — Photomicrograph of primary melt inclusion in a clinopyroxene host mineral from Sab38 granulite xenolith. **g** — Photomicrograph of primary melt inclusions in plagioclase host mineral from Sab38 granulite xenolith. **h** — Backscattered electron image of a primary silicate melt inclusion in ilmenite host mineral from Sab38 granulite xenolith.

were published by Németh et al. (2015). Here we present only the main features. Xenolith Sab38 is layered, whereas the xenolith Mi26 shows a "patchy" microtexture (Fig. 2c), but both share a migmatitic texture with garnet–clinopyroxene–orthopyroxene–plagioclase-bearing melanosome and a clinopyroxene-bearing plagioclase-rich leucosome (Fig. 2c and d). Both xenoliths show mostly curved grain boundaries with irregular mineral shapes and many symplectitic reaction domains. This was interpreted as non-equilibrium microtexture in Németh et al. (2015), which is a fundamental difference compared to the other studied xenoliths from the area. Among accessory phases, orthopyroxene (only in Sab38 xenolith), titanite, apatite, zircon, and opaque minerals (mostly ilmenite) were also identified.

In the Sab38 xenolith, the clinopyroxene+plagioclase-bearing leucosome contains quartz as an accessory mineral. Garnets are mostly resorbed kelyphitic remnants (Fig. 2c and d) or sometimes symplectitic pseudomorphs (Supplementary Fig. S1) of plagioclase–orthopyroxene–spinel with rare relict garnet. The breakdown of titanite to clinopyroxene–ilmenite±plagioclase symplectites (Fig. 2d and Suppl. Fig. S2) is observed frequently at the contact between the SMI-free melanosome (wall rock) and the plagioclase-rich inclusion-bearing leucosome domains. Thin melt films along the grain boundaries (Fig. 2e and Suppl. Fig. S2) and glassy melt pockets from the infiltrating alkaline basalt are also observed.

Silicate melt inclusion petrography

Both Sab38 and Mi26 xenoliths contain the same types of SMIs, in the same SMI-bearing minerals (clinopyroxene, plagioclase, and ilmenite) with similar appearances (Suppl. Table S1). Two types of primary SMIs coexist in plagioclase (Fig. 2e): a colourless glass dominated (70–100 vol. %) SMI (type G) and a volatile dominated black SMI with a low amount of glass (up to 20 vol. %) referred to as type V silicate melt inclusion. The G type SMIs have a size between 15–30 μm, sometimes up to 100 μm. These SMIs consist of a colourless glass phase+bubble(s), have a negative crystal shape and their boundary is slightly ragged (Fig. 2g). The vapour bubble (up to 30 vol. %) in the plagioclase hosted SMIs is dark and consists of one phase at room temperature (Fig. 2g). The vapour dominated type V SMIs have also a negative crystal shape. Their size ranges between 20 and 50 μm. These SMIs always show a decrepitation halo. The SMIs trapped in clinopyroxene contain mostly brown glass (95–100 vol. %). They are also always decrepitated (Fig. 2f) and their size is usually between 20–30 μm. These SMIs usually contain one bubble (up to 5 vol. %) with two fluid phases (liquid and vapour) at room temperature (Fig. 2f). The liquid phase occupies about 60 vol. % of the bubble. The ilmenite trapped SMIs were detected only by SEM. Their size is around 30 μm. These SMIs have rounded or oval shapes with no visible sign of decrepitation (Fig. 2h) and consist of glass±bubble (up to 10 vol. %) (Fig. 2h).

Major element analyses of the glass phase in SMIs

Most of the glass in the plagioclase and clinopyroxene hosted SMI is dacitic, trachydacitic, or rhyolitic in composition, whereas the ilmenite hosted SMIs are more scattered over a wide range in composition from trachybasaltic to trachydacitic (Fig. 3a and c). The glassy SMIs trapped in clinopyroxene in the Mi26 xenolith have an average FeO-content of 5.7 wt. % (Figs. 4a,c and 5a). Their MgO-content is 0.8 wt. % and their K_2O/Na_2O is around 3.0 (Figs. 4b,d, 5b and Suppl. Table S2). The clinopyroxene hosted SMIs in the Sab38 xenolith show an average FeO-content of 4.7 wt. % (Figs. 4a,c and 5a), whereas their MgO-content is 0.1 wt. % and K_2O/Na_2O is around 2.2 (Figs. 4b,d, 5b and Suppl. Table S2).

The plagioclase-hosted SMIs in the Mi26 granulite xenolith show an average FeO-content of 1.5 wt. % (Figs. 4a,c and 5a), their MgO-content is 0.2 wt. %, whereas their K_2O/Na_2O ratio is around 1 (Figs. 4b,d, 5b and Suppl. Table S2). In contrast, in the Sab38 granulite xenolith, the plagioclase hosted SMIs have an average FeO-content of 6.3 wt. % (Figs. 4a,c and 5a), their MgO-content is 0.7 wt. % and their K_2O/Na_2O ratio is around 1.2 (Figs. 4b,d, 5b and Suppl. Table S2).

The ilmenite hosted SMIs in Mi26 granulite contain much lower amounts of SiO_2 (45.9–54.3 wt. %) than in Sab38 granulite (60.1–62.5 wt. %) (Fig. 3a,c and Suppl. Table S2). The FeO-content is much higher (17.0–22.0 wt. %) in the glass of the ilmenite hosted SMIs in the Mi26 xenolith than in Sab38 granulite (7.0–9.0 wt. %; Fig. 5a). The Na_2O-content is lower in SMIs from the Mi26 granulite (1.6–2.2 wt. %) compared to those in Sab38 granulite (2.4–3.7 wt. %), whereas the K_2O-content is almost the same in the SMIs from both xenoliths (Mi26: 3.6–4.2 wt. %; Sab38: 3.9–4.2 wt. %) (Fig. 5b).

Trace element composition of mineral phases

All plagioclases in both samples have similar trace element pattern regardless of their location (Fig. 6a,b and Suppl. Table S2). The SMI-bearing plagioclases show LILE (large ion lithophile element) enrichment, especially in Cs and Rb, compared to the SMI-free plagioclases, when normalized to the primitive mantle (Sun & McDonough 1989) (Fig. 6f). The trace element content of the plagioclase is enriched in light rare earth elements (LREE) compared to heavy REEs, with positive Eu anomalies (Fig. 6a and b).

Clinopyroxenes that contain SMIs are enriched in LILE (especially Cs) compared to SMI-free clinopyroxenes in both xenoliths (Fig. 6c and d). All clinopyroxenes are enriched in LREE relative to HREE (heavy rare earth element) (Fig. 6c,d and Suppl. Table S2). However, there is a variation of La/Yb ratios in both xenoliths (1.26±0.71 in the Mi26 granulite xenolith and 1.42±1.29 in the Sab38 xenolith, respectively, normalized to the average lower crust of Rudnick & Gao 2003). In addition, all analysed clinopyroxene show negative Eu anomaly ($Eu_N/Eu^*_N < 1$ normalized to the average lower crust), but the degree of this anomaly is different
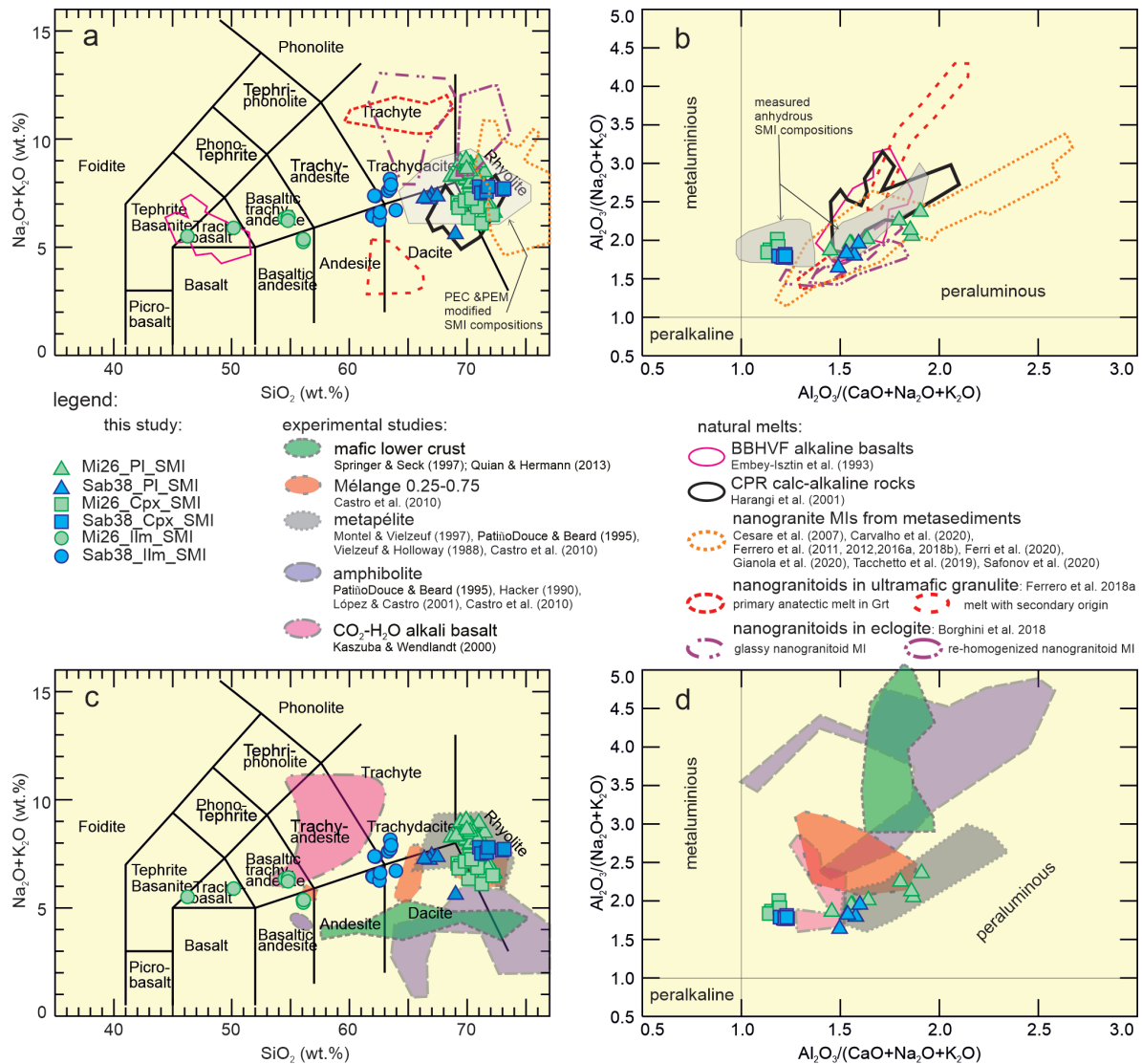
Fig. 3. The genetic processes of the silicate melt inclusions according to their chemical composition with major element variations compared to natural melts and rocks (a and b) and to experimental melts (c and d). Fig. 3b and d shows the corrected composition of the silicate melt inclusions according to the post entrapment processes. For more details, see section "Reconstruction of the major element composition of SMIs". Mineral abbreviations follow Kretz (1983). **a** — Total alkali–silica (TAS) diagram for variation of silicate melt inclusion composition trapped in plagioclase, clinopyroxene and ilmenite from Mi26 and Sab38 granulite xenoliths, respectively compared to natural melts and rocks. **b** — A/CNK–A/NK diagram showing the peraluminous affinity of the studied SMIs compared to natural melts and rocks. **c** — Total alkali–silica (TAS) diagram for variation of silicate melt inclusion composition trapped in plagioclase, clinopyroxene and ilmenite from Mi26 and Sab38 granulite xenoliths, respectively compared to experimental melts. **d** — A/CNK–A/NK diagram showing the peraluminous affinity of the studied SMIs compared to experimental melts.

(Fig. 6c, d and e). Two clinopyroxene groups can be distinguished in the Sab38 xenolith based on the Eu anomaly and the La/Yb ratio (Fig. 6e), which do not completely coincide with petrographic features. One of the clinopyroxene groups shows a high La/Yb ratio (2.46–4.74) with a smaller Eu anomaly ($Eu_N/Eu^*_N = Eu/(Sm*Gd)^{0.5} = 0.65$–0.99). SMI-free clinopyroxenes belong to this group. They occur either in the garnet-bearing melanosome or the plagioclase-rich leucosome segment. The other clinopyroxene group consists of clinopyroxene with a low La/Yb ratio (0.52–1.22) and a larger Eu anomaly ($Eu_N/Eu^*_N = 0.23$–0.54). Clinopyroxenes, which belong to this group, appear mostly in the clinopyroxene–

plagioclase-rich leucosome assemblage from the Sab38 xenolith and contain SMIs. Some inclusion-free clinopyroxene from the plagioclase-rich assemblage also belongs here as well as some clinopyroxene from the wall-rock (Fig. 6e). Similar groups cannot be distinguished in the Mi26 xenolith. The clinopyroxene compositions predominantly plot between the values of the two observed groups from the Sab38 xenolith (Fig. 6e). However, the group characterized by a noticeable Eu anomaly and small La/Yb ratio is also significant and mostly appears in SMI-bearing minerals within the clinopyroxene–plagioclase-rich pockets of the xenolith.

Trace element composition of SMIs

The multicomponent trace element patterns of silicate melt inclusions (Fig. 7a,c and e) are broadly similar regardless of the host minerals. The exceptions are the SMI trapped in ilmenite with positive Nb and Ta anomalies caused by additional signals from ilmenite (Fig. 7e). Caesium, Rb, Th, U, and Pb show positive anomalies, but Ba, Nb, Ta, and Sr shows minima with negative anomalies relative to the adjacent elements (Fig. 7a,c,e and Suppl. Table S2). Additionally, there is a significant negative Zr anomaly in the SMIs in some Sab38 plagioclases (Fig. 7a). The REE pattern of the SMIs (Fig. 7b, d and f) show a steady decrease from La to Lu in all the host minerals.
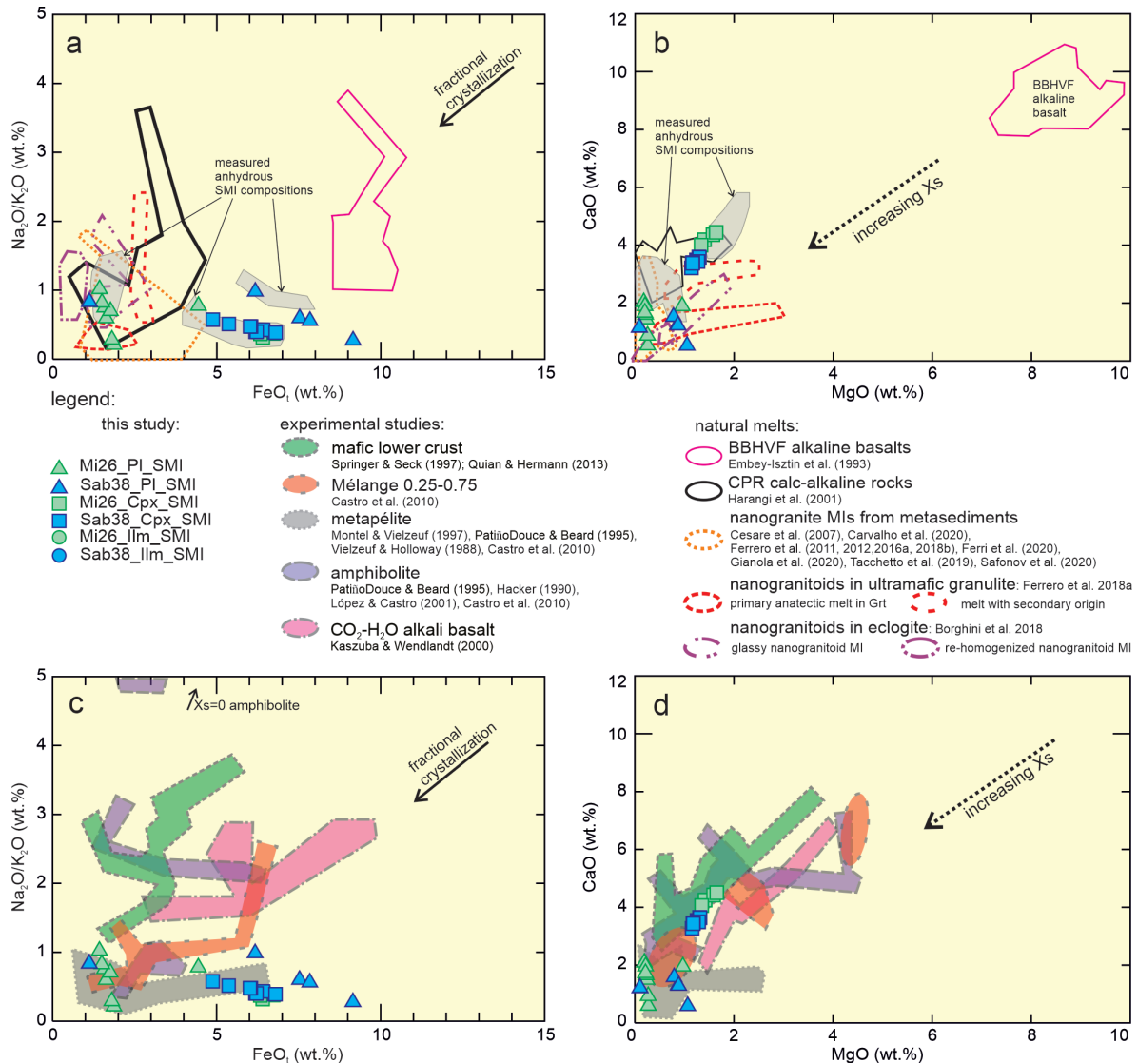
Fig. 4. The genetic processes of the silicate melt inclusions according to their post entrapment processes corrected chemical composition with major element variations compared to natural melts and rocks (a and b) and to experimental melts (c and d). For more details, see section "Reconstruction of the major element composition of SMIs". Mineral abbreviations follow Kretz (1983). **a** — Na_2O/K_2O–FeO_{tot} diagram shows that alkaline basalts from the Bakony–Balaton Highland Volcanic Field (BBHVF) cannot be the source of the silicate melt inclusions. Also, only a part of the plagioclase hosted silicate melt inclusions show similarities to the calc-alkaline rock from the northern Pannonian Basin, just as to the eclogite and metasediment hosted natural nanogranitic melts. The long black arrow shows how the fractional crystallization of a clinopyroxene–plagioclase assemblage changes the melt composition. **b** — MgO–CaO diagram also shows that alkaline basalts from the Bakony–Balaton Highland Volcanic Field cannot be the source the studied silicate melt inclusions, and the inclusions fits to the composition of the calc-alkaline rocks from the northern Pannonian Basin. Also, only a part of the plagioclase hosted silicate melt inclusions show similarities to the ultramafic, eclogite and metasediment hosted natural nanogranitic melts. **c** — Na_2O/K_2O–FeO_{tot} diagram shows that neither pure amphibolite nor pure metasediment cannot be the source of the silicate melt inclusions. Xs means the ratio of the sediments in the starting material of the experimental melts. The long black arrow shows how the fractional crystallization of a clinopyroxene-plagioclase assemblage changes the melt composition. **d** — MgO–CaO diagram shows that the clinopyroxene hosted silicate melt inclusions are more primitive than the plagioclase hosted ones. Xs means the ratio of the sediment in the starting material from the mélange and the arrow shows the increase of this ratio towards the pure metasedimentary starting material.

The concentration of some REEs (Nd, Sm, Eu, Yb) was below the detection limit in some SMIs with smaller size (Suppl. Table S2). To complement the lack of REE concentrations in the clinopyroxene hosted SMIs, we determined the $^{Cpx/melt}K_D$ for those elements. The distribution of the trace elements between clinopyroxene and the melt is influenced in SiO_2-rich melts both by the structure of the clinopyroxene and the structure of the melt (Gaetani 2004; Huang et al. 2006). Therefore, we used distribution coefficients to determine equilibrium melt compositions from those experimental studies in which the composition of the melt and the clinopyroxene is the closest to the one we measured (Huang et al. 2006). By these values (Suppl. Table S2), it is now possible to determine REE patterns and ratios. The La^N/Yb^N ratio (normalized to C1 chondrite) is highly variable (av=18.17±10.77) and it shows a wider range in the Mi26 xenolith (4.51–45.78) than in the Sab38 xenolith (6.57–23.53). Otherwise, REE concentrations show a decrease from La to Lu with a negative Eu anomaly (Fig. 7d).
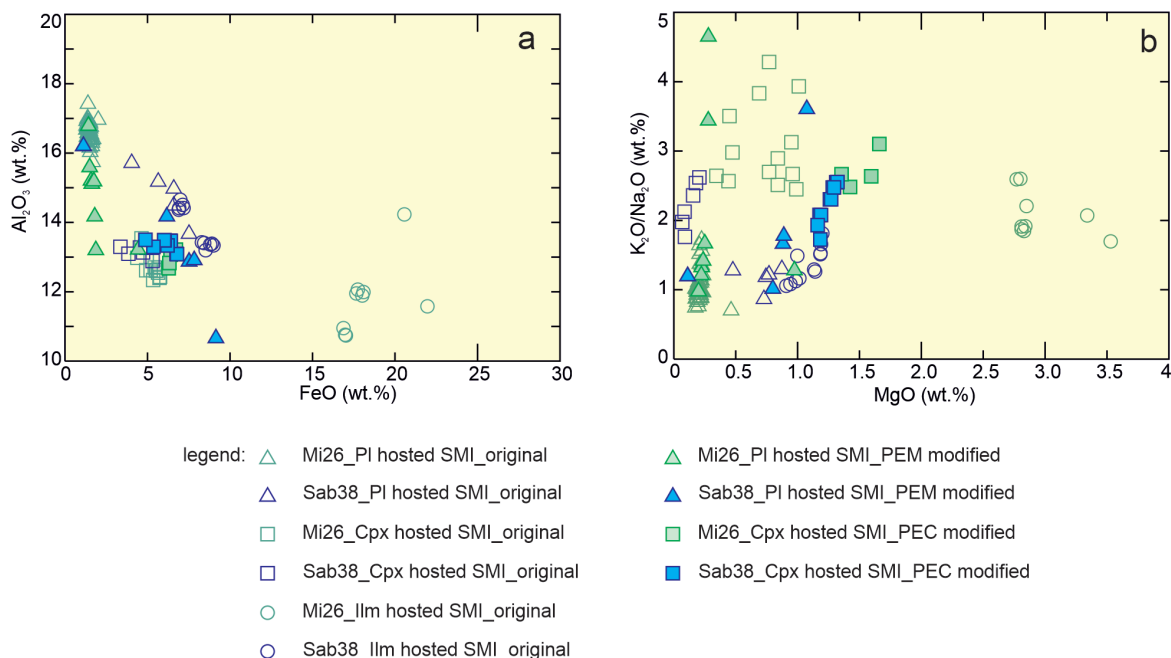
Reconstruction of the major element composition of SMIs

Petrographic observations (Fig. 2) showed that the edges of some melt inclusions are ragged, and clinopyroxene hosted melt inclusions are decrepitated. These suggest potential chemical modifications of the silicate melt after entrapment. Based on SMI compositions, and their host minerals, it is clear that many of the SMIs are not in chemical equilibrium with their host (e.g., $K_D(Ab–An)^{Pl-melt}$ ranges from 0.11 to 0.23). Therefore, in order to reconstruct the composition of the primary melt inclusions at the time of entrapment, we needed to correct the melt compositions for post entrapment processes.

Post entrapment changes in the composition of the glass can be caused by crystallization or melting. The post entrapment crystallization means that even the melt inclusions seem to be glassy, partial crystallization of the host mineral occurred on the wall of the inclusion in a few vol. % (e.g., Steele-Macinnis et al. 2011). For the correction, one must add the composition of the host mineral back into the composition of the silicate melt inclusion. However, post entrapment melting means the opposite process, when host mineral was added into the glass of the silicate melt inclusion due to high temperature, e.g., when the alkaline basalt brought up the xenoliths. This melting process can be corrected by subtraction of the composition of the host mineral from the composition of the silicate melt inclusion (e.g., Halter et al. 2004; Rasmussen et al. 2018).

Post entrapment crystallization (PEC) and post entrapment melting (PEM) calculations were applied in the SMIs from clinopyroxene and plagioclase (Suppl. Table S3), which had complementary analyses adjacent to the SMIs in their host mineral (on an average 20 µm from the SMI) and coherent but more distant points were also analysed in the same mineral (>30 µm from the SMI). Mineral compositions analysed adjacent to the melt inclusions were added back or extracted from the silicate melt compositions until chemical equilibrium was

Fig. 5. Major element composition of the silicate melt inclusions. The raw data (empty symbols) is compared to the post entrapment melting (PEM) and post entrapment crystallization (PEC) modified compositions (filled symbols) of the silicate melt inclusion showing the compositional change. Post entrapment modifications are based on mineral/liquid partition coefficients of Putirka (2008). Mineral abbreviations follow Kretz (1983). **a** — FeO_{total}–Al_2O_3 diagram shows that the plagioclase hosted silicate melt inclusions show higher compositional variation compared to the clinopyroxene hosted silicate melt inclusions. The PEM corrections resulted in a higher Al-content in the plagioclase hosted inclusions whereas the PEC correction resulted in a higher Fe-content in the clinopyroxene hosted silicate melt inclusions. **b** — MgO–K_2O/Na_2O diagram shows that clinopyroxene hosted silicate melt inclusions have higher MgO-content than the plagioclase hosted ones. The K_2O/Na_2O ratio shows differences between the composition of the glass of the melt inclusions in the different host minerals.
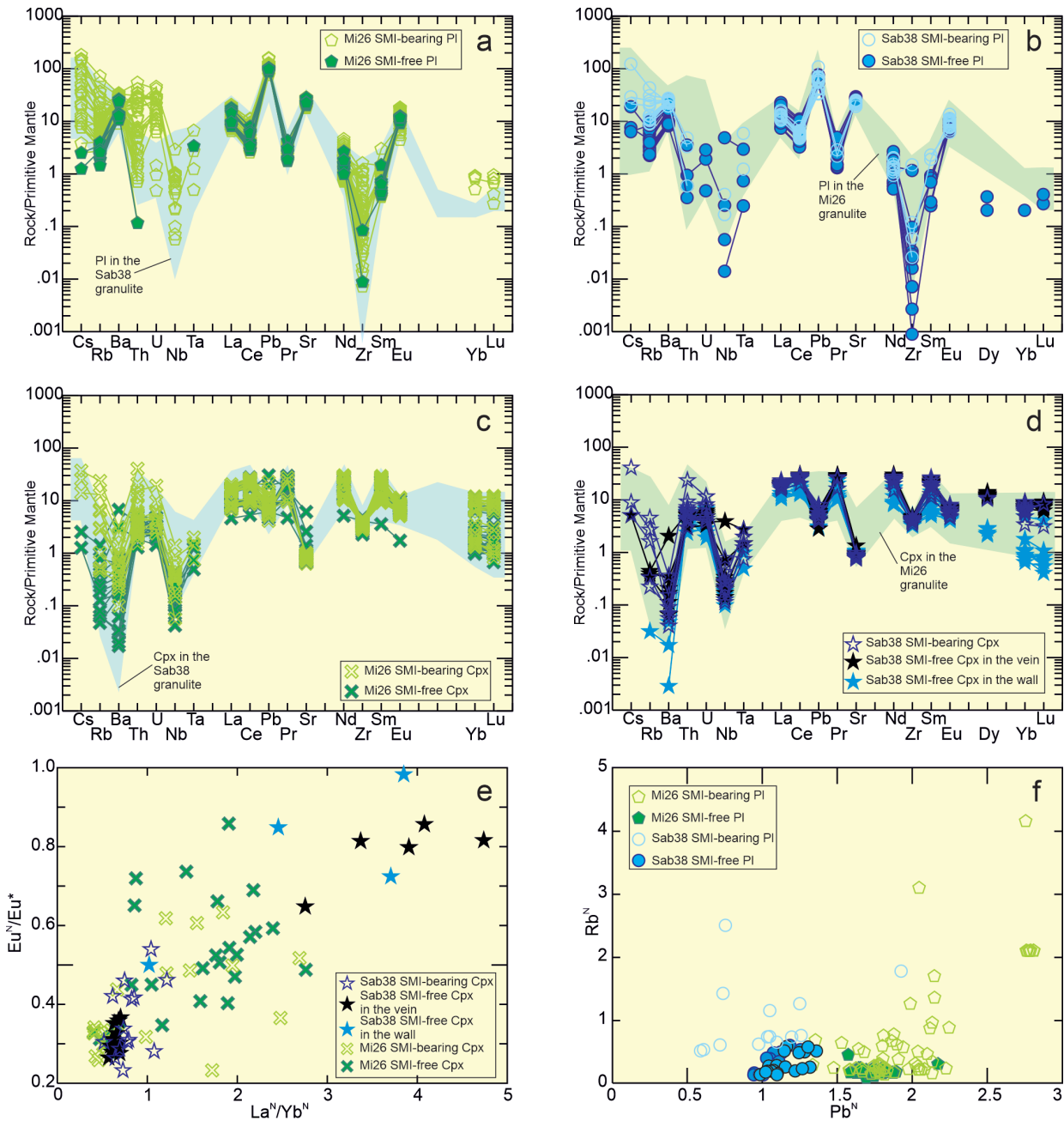
Fig. 6. Trace element distributions in the minerals. Symbols with green colour belong to the Mi26 granulite xenolith, and symbols with blue stand for the Sab38 granulite xenolith. Mineral abbreviations follow Kretz (1983). **a** — Trace element distribution in plagioclases from the Mi26 granulite xenolith normalized to the primitive mantle (PM, Sun & McDonough 1989). The light blue area in the background represents the composition of the plagioclases in the Sab38 granulite xenolith. **b** — Trace element distribution in plagioclases from the Sab38 granulite xenolith normalized to PM. The light green area in the background represents the composition of the plagioclases in the Mi26 granulite xenolith. **c** — Trace element distribution in clinopyroxenes from the Mi26 granulite xenolith, normalized to PM. The light blue area in the background represents the composition of the clinopyroxenes in the Sab38 granulite xenolith. **d** — Trace element distribution in the clinopyroxenes from the Sab38 granulite xenolith, normalized to PM. The light green area in the background represents the composition of the clinopyroxenes from the Mi26 granulite xenolith. **e** — La/Y vs Eu anomaly ($Eu_N/Eu*_N=Eu/(Sm*Gd)^{0.5}$) diagram (normalized to average lower crust Rudnick & Gao 2003). **f** — LILE enrichment in the SMI-bearing plagioclases normalized to average lower crust (Rudnick & Gao 2003).

achieved between the silicate melt and the host mineral analysed further away from the SMI.

In SMIs trapped in clinopyroxene the equilibrium criteria was $(K_D(Fe–Mg)^{Cpx-melt})=0.27\pm0.03$ based on Putirka (2008), which is the most suitable model for these melt compositions. The SMIs trapped in clinopyroxene are broadly in chemical

equilibrium with their host minerals from the Mi26 granulite xenolith, but the equilibrium K_D of 0.27 is best matched with 5 % post entrapment crystallization (PEC) recalculation (Suppl. Table S3). In the Sab38 xenolith, the SMIs in clinopyroxene are not in chemical equilibrium with their host mineral but can be corrected with up to 10 % PEC calculation. After this
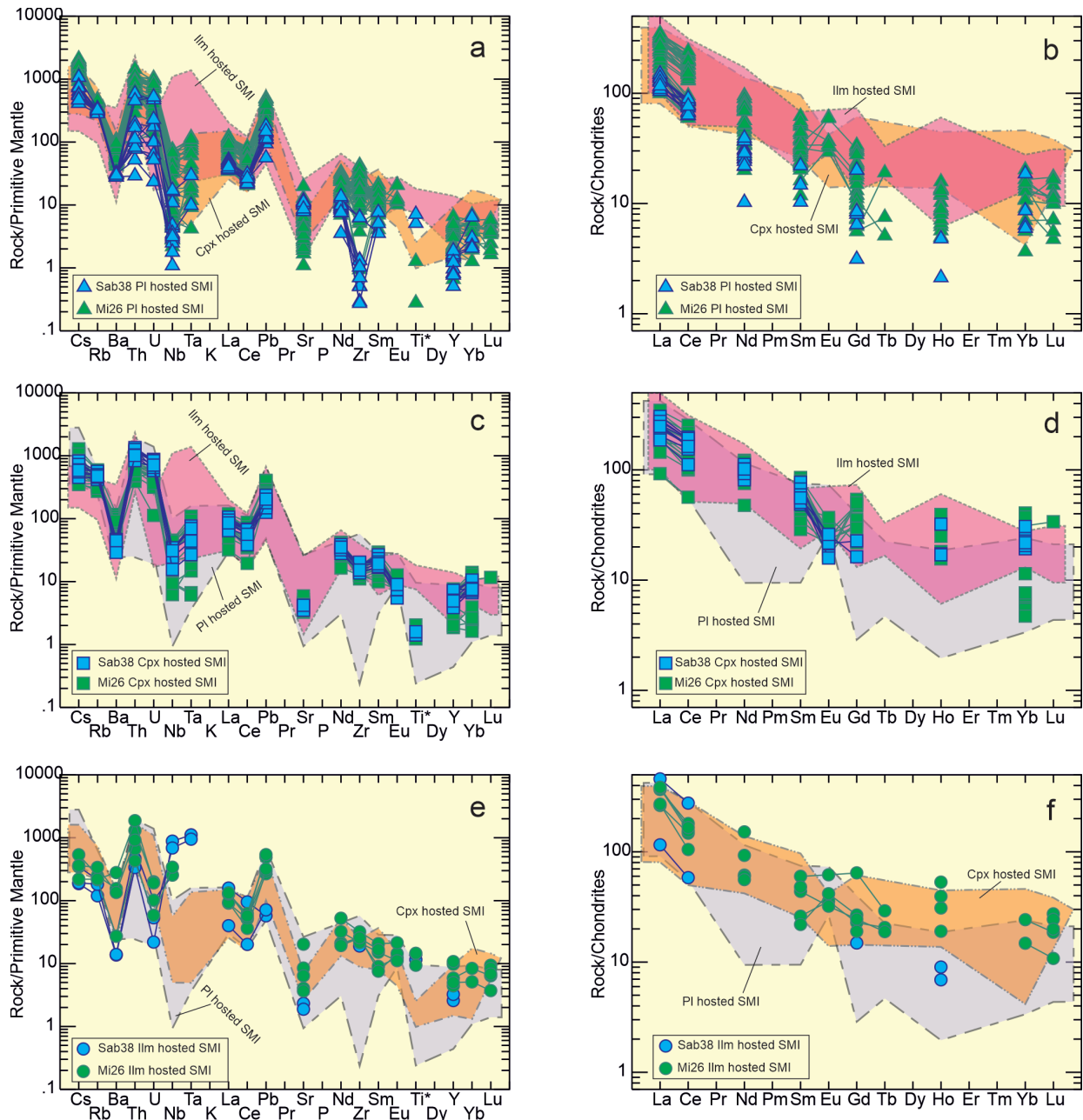
Fig. 7. Trace element distribution in silicate melt inclusions normalized to the primitive mantle and to chondrites (Sun & McDonough 1989). The triangles mark the plagioclase hosted silicate melt inclusions, while the squares stand for clinopyroxene hosted ones, and the circles stand for ilmenite hosted silicate melt inclusions. The coloured patterns in the background show the composition of the silicate melt inclusions trapped in the other two host minerals. Lilac belongs to plagioclase hosted silicate melt inclusions, orange to the clinopyroxene hosted silicate melt inclusions, and magenta to the ilmenite hosted ones. Mineral abbreviations follow Kretz (1983). **a** — Multi-element diagram of trace elements in the plagioclase hosted silicate melt inclusions in the Mi26 and Sab38 granulite xenoliths. **b** — REE diagram of the plagioclase hosted silicate melt inclusions with the same colour code as in Fig. 7a. **c** — Multi-element diagram of trace elements in clinopyroxene hosted silicate melt inclusions in the Mi26 and Sab38 granulite xenoliths. **d** — REE diagram of clinopyroxene hosted silicate melt inclusions with the same colour code as in Fig. 7c. **e** — Multi-element diagram of trace elements in ilmenite hosted silicate melt inclusions from the Mi26 and Sab38 granulite xenoliths. **f** — REE diagram of plagioclase hosted silicate melt inclusions with the same colour code as in Fig. 7e.

correction, the chemical composition of the SMI hosted in clinopyroxene is similar to the ones trapped in clinopyroxene in the Mi26 xenolith (Figs. 3, 4 and 5).

The partition coefficient in plagioclase hosted SMIs was calculated based on $K_D(Ab–An)^{Pl-melt}$ from Putirka (2008), which should be in the range of 0.1±0.05 for temperatures

<1050 °C. The SMIs and their host plagioclase show a wide range in their K_Ds (0.11–0.23) (Suppl. Table S3). Considering that the equilibrium temperature based on clinopyroxene-melt thermometry, presented in section 4.6., is close to 940 °C (Putirka 2008), we suggest that the majority of the plagioclase hosted SMIs are not in equilibrium with their host mineral,

because the $K_D(Ab–An)^{Pl-melt}$ values are beyond 0.15. We suggest that most SMIs suffered post entrapment plagioclase melting (PEM) from the wall of the SMIs, which led to high $K_D(Ab–An)^{Pl-melt}$ values. We extracted plagioclase from the SMIs to reach the equilibrium $^{Pl/melt}K_D$ relevant for T<1050 °C (0.05–0.15). This needed 5 to 40 % plagioclase extraction (Suppl. Table S3).

The SMIs in ilmenite were not corrected as there are no available equilibrium criteria to assess post entrapment processes for this mineral. The melt composition of the SMIs after PEC and PEM calculations suggests that all the inspected SMIs trapped in clinopyroxene and plagioclase in both xenoliths have a peraluminous composition (Fig. 3b and d). However, clinopyroxene hosted SMIs show the least peraluminous compositions and have slightly higher MgO content (Figs. 4 and 5) compared to plagioclase hosted ones.

Results of mineral-melt thermobarometry

We calculated equilibrium pressure (p, based on Putirka et al. 2003) and temperature (T based on Putirka 2008) conditions for the crystallization of SMI-bearing minerals. We used PEC and PEM corrected melt inclusion compositions and the composition of the host minerals analysed further away from the SMI for this calculation. In the Mi26 granulite xenolith, the clinopyroxene hosted SMIs give a 937±5 °C equilibrium temperature and a 3.7±0.4 kbar pressure (Suppl. Table S3, see below). In the Sab38 granulite xenolith, the clinopyroxene hosted SMIs give a 931±9 °C equilibrium temperature (Putirka 2008) and a 5.6±0.3 kbar pressure (Putirka et al. 2003). The variation in the calculated T and p is significantly smaller than the uncertainty of the thermobarometer's calibration (±45 °C and ±1.7 kbar).

In the case of SMIs trapped in plagioclase, the mineral-melt pairs suggest 864±36 °C based on Putirka (2008) in Mi26 granulite. In these conditions, the melt contained 4.5±0.6 wt. % H_2O (Suppl. Table S3). For the Sab38 xenolith, 871±43 °C was calculated. The derived H_2O content is 3.3±0.2 wt. %. A similar H_2O-content was calculated in the case of the plagioclase hosted SMIs based on Devine et al. (1995) with 3.0±0.9 wt. % in the Mi26 granulite xenolith and 3.3±1.4 wt. % in Sab38 granulite xenolith, respectively (Suppl. Table S2). Note that the temperature estimates based on plagioclase-melt pairs have higher variations (1 σ stdev) than the calibration uncertainty (±36 °C in Putirka 2008). Also, the temperatures derived by plagioclase-melt thermometry are lower and vary significantly compared to those obtained by clinopyroxene-melt thermometry.

Discussion

Characteristics of the metasomatizing melt

The composition of the SMIs reconstructed by PEC and PEM calculations (Suppl. Table S3) suggests that clinopyro-

xene and plagioclase hosted SMIs in both xenoliths have peraluminous composition (Fig. 3b and d). Clinopyroxene hosted SMIs show slightly higher MgO content (Figs. 4 and 5) compared to plagioclase hosted ones. Furthermore, the clinopyroxene crystallization temperatures are higher and cover a much smaller range than those calculated for plagioclase (Suppl. Table S3). This suggests that clinopyroxene might have crystallized before plagioclase in the leucosome and their SMIs might be more representative of the original metasomatic melt than those trapped in plagioclase.

The composition of the PEC and PEM corrected SMIs were compared with the composition of nanogranite SMIs (collected in Nicoli & Ferrero 2021) formed in similar p–T conditions as described for mafic garnet granulite xenoliths from the BBHVF. The relevant inclusions were all in rocks with metasedimentary origin (Cesare et al. 2007; Ferrero et al. 2011, 2012, 2016, 2018b; Tacchetto et al. 2019; Carvalho et al. 2020; Ferri et al. 2020; Gianola et al. 2020; Safonov et al. 2020). Figure 4a shows that these nanogranite inclusions are similar to the plagioclase hosted SMIs, whereas the inclusions trapped in Cpx have different characteristics with lower SiO_2-, higher FeO- and CaO-contents, as well as the Cpx hosted SMIs are the least peraluminous ones (Figs. 3b, 4a and b). The ultramafic granulite (Ferrero et al. 2018a) and the eclogite hosted (Borghini et al. 2018) nanogranite inclusions show very little or no overlap (Figs. 3a,b and 4a,b) with the composition of the studied SMIs. In the TAS diagram the composition of Cpx hosted SMIs fall between the compositional fields of nanogranites with metasedimentary and ultramafic origin (Fig. 3a).

The major element composition of clinopyroxene hosted SMIs is similar to melts derived by partial melting of biotite–quartz–plagioclase mineral assemblages from metagreywackes or gneiss (Vielzeuf & Montel 1994; Patiño-Douce & Beard 1995; Montel & Vielzeuf 1997; Figs. 3c,d, 4c,d and Suppl. Table S2). The composition of the SMIs differs from melts, which originated by partial melting of mafic granulite or quartz amphibolite since they have low alkali contents and a higher Na_2O/K_2O ratio (Hacker 1990; Springer & Seck 1997; Figs. 3c and 4c). The chemical compositions of SMIs also resemble that of the silicate melts produced by melting of a metabasalt–metasediment mélange (Castro et al. 2010; Figs. 3c,d and 4d). If we assume that a metasedimentary source contained biotite and/or K-feldspar minerals, these minerals had to be consumed during the partial melting process. Biotite relics in orthopyroxenes and garnets in the presence of CO_2-dominated fluid inclusions in granulite xenoliths were observed from the same localities.

SMIs trapped in clinopyroxene are also characterized by positive LILE such as Cs and Rb, and negative HFSE anomalies (Figs. 7c,d and 8b,c). The HFS anomaly can be explained by the presence of residual hornblende or a Ta–Nb–Ti-bearing phase, such as rutile, ilmenite, or titanite, during the partial melting (Qian & Hermann 2013). In the studied granulite xenoliths, ilmenite appears as accessory phase, moreover, it contains SMIs (Fig. 2). The elevated U and especially Th

concentrations in the SMIs (Fig. 7a, c and e) and their host relative to the SMI-free granulitic minerals (Suppl. Table S2), might be consistent with the presence of metapelitic component in the melt (Ewing et al. 2014). Such melts are typical for magmas from island arc volcanism (e.g., Saunders et al. 1991).

Evidence of melt-wall-rock interactions

Plagioclase hosted SMIs

Most of the SMIs in plagioclase (and ilmenite) are predominantly characterized by lower Yb-content and higher Ce/Yb ratio (Fig. 8a) as well as higher Al_2O_3-content than those trapped in clinopyroxene (Figs. 3b and 5a). However, some SMIs trapped in plagioclase (and ilmenite) (Fig. 7) show chemical compositions in both xenoliths similar to those observed in the clinopyroxene hosted ones. This chemical difference and the large variation in composition (Fig. 7) suggest that the plagioclase (and ilmenite) hosted melt inclusions represent reaction products during trapping in their host minerals after a various degree of interaction between the original melt and granulite wall rock. The reactant wall rock, which is now garnet-free, however, contains clinopyroxenes that preserved the chemical characteristics being in equilibrium with garnet (high La/Yb ratios and the lack of significant negative Eu-anomaly, Fig. 6e) as REE diffusive re-equilibration under lithospheric conditions is very slow (Van Orman et al. 2001). The low and variable plagioclase crystallization temperatures (Suppl. Table S3) support a prolonged reaction between the original metasomatic melt and the granulite wall rock.

Ilmenite–clinopyroxene±plagioclase symplectites

The dominant nonequilibrium texture of these xenoliths with the presence of ilmenite–clinopyroxene±plagioclase symplectites and the resorbed pseudomorphs after garnet, next to the SMI-bearing plagioclase-rich domains, all indicate reactions initiated by the infiltrating melt/fluid noted in Németh et al. (2015). Clinopyroxene–ilmenite symplectites (Suppl. Figs. S1, S2) are quite common in lower crustal mafic garnet granulite xenoliths and in garnet-pyroxenites from the BBHVF. Occasionally, titanite inclusions can also be observed in the symplectites (Suppl. Fig. S1). We demonstrate with mass-balance calculations (Suppl. Table S4) that
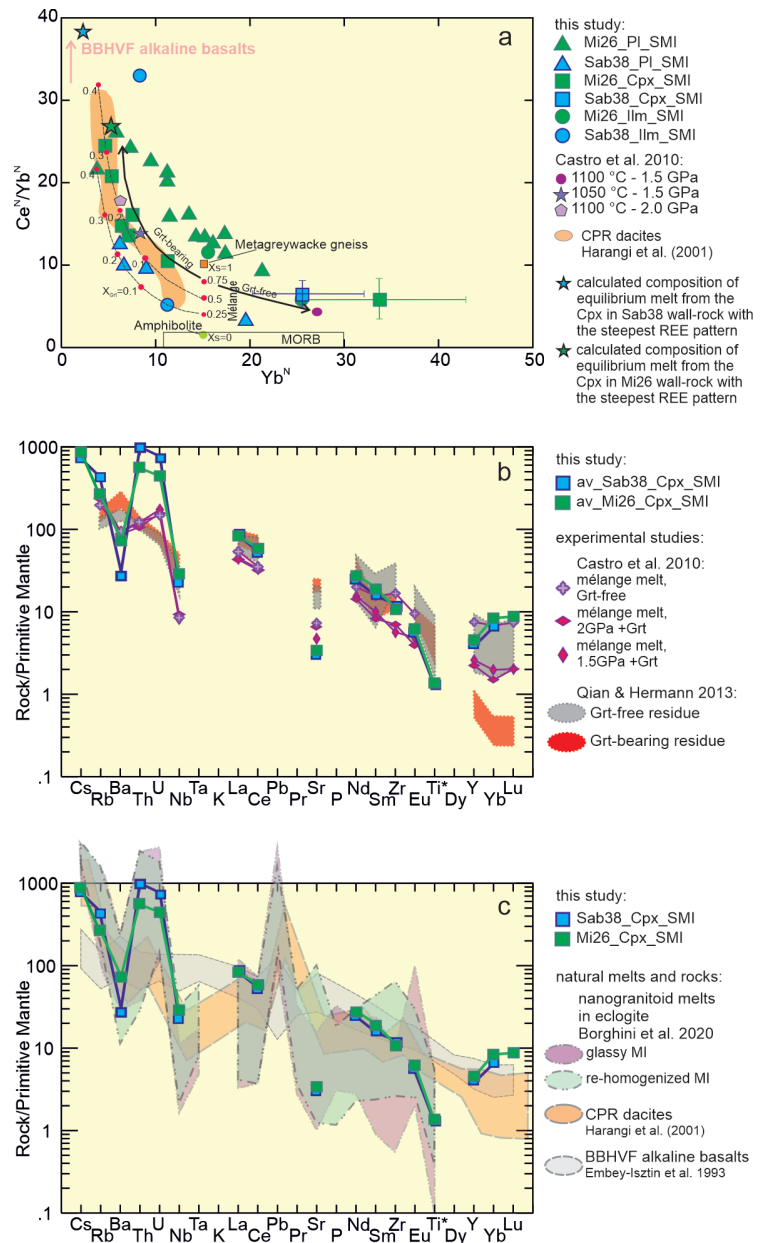
Fig. 8. Origin of the metasomatizing melt based on trace element distributions. The considered earliest composition of the melt trapped in clinopyroxenes suggests a hybrid origin by melting of a metasediment-metabasalt mélange leaving behind a garnet-free residuum. **a** — Yb(N) vs Ce/Yb(N) diagram normalized to C1 (Sun & McDonough 1989) suggests the melting of a mélange with 50–75 % metasediment and 25–50 % amphibolite composition is responsible for the formation of the silicate melt now trapped in clinopyroxene. The silicate melt inclusions trapped in plagioclase and ilmenite host minerals show a nearly continuous change in their composition with a small Yb concentration and a high Ce/Yb ratio. They represent varying degrees of re-equilibration between the original metasomatizing melt and the wall rock that contains clinopyroxenes preserving the equilibrium REE composition with garnets now present as symplectites. **b** — This diagram shows the trace elements pattern of the clinopyroxene hosted silicate melt inclusions compared to those of the experimental melts in equilibrium with various residual mineral assemblages with or without garnet. The best match is observed with a melt composition that leaves behind a garnet-free residuum (Castro et al. 2010; Qian & Hermann 2013). The Ti* was calculated from the major element data. **c** — This diagram shows the trace elements pattern of the clinopyroxene hosted silicate melt inclusions compared to those of the natural melts in eclogite (Borghini et al. 2020) and natural rocks from the Pannonian Basin (Embey-Isztin et al. 1993; Harangi et al. 2001).

the composition of the clinopyroxene–ilmenite±plagioclase symplectites differs from that of the titanites. When clinopyroxene and ilmenite are mixed in the proportion, observed in the symplectites, the amount of Fe and Mg and Al is too high compared to the composition of titanite, whereas the Ti and Ca content is too low (Suppl. Table S4). The addition of plagioclase surrounding the clinopyroxene–ilmenite intergrowth changes the bulk symplectite composition by increasing the Al, the alkaline elements, and the Si contents as well (Suppl. Fig. S2). Therefore, we suggest the following reaction for symplectite formation in these xenoliths:

$$\text{titanite} + \text{melt} = \text{Cpx} + \text{Ilm} + \text{Pl} + \text{melt2} \tag{1}$$
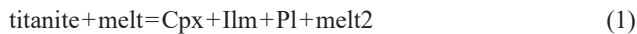
in which the felsic melt1 facilitates the formation of symplectites by adding heat, alkalis, SiO_2 and possibly H_2O, whereas melt2 might transports away primarily CaO and TiO_2 from the symplectites and may be similar to those observed as melt inclusions in ilmenite.

Evolution of the crustal domain represented by the granulite xenoliths

The dominantly non-equilibrium microtexture of the garnet granulite xenoliths with a few equilibrium domains is different from the previously described lower crustal granulites from the region (Török 1995; Dégi & Török 2003; Török et al. 2005; Dégi et al. 2009, 2010). Although most of the lower crustal mafic granulites show equilibrium microtextures, locally some disequilibrium domains representing later reactions. These are resorbed relics of hydrous minerals in nominally anhydrous ones in the presence of CO_2-rich fluid inclusions which are signs of dehydration melting of hydrous minerals (amphibole and biotite, or kelyphitic coronas as breakdown reactions of garnet, Dégi et al. 2010). In the studied xenoliths, the observed few equilibrium domains in the Mi26 and Sab38 xenoliths contain garnet–clinopyroxene–plagioclase assemblage, which represents a former equilibrium garnet granulite (Fig. 9 – t1 step). These domains equilibrated at 1.2 GPa pressure (~45 km) and 820–930 °C temperatures in our samples (Németh et al. 2015). This fits the p–T interval of 1.0–1.6 GPa and 800–1000 °C, deduced from mafic garnet granulite xenoliths with similar mineralogy (Török et al. 2005). According to Raman and IR spectroscopy, this mineral assemblage is water-free and contains CO_2-dominated±CO+H_2S fluid in Pl hosted pseudosecondary fluid inclusions (Németh et al. 2015). These domains are remnants of the thick crust that characterized the region before crustal extension.
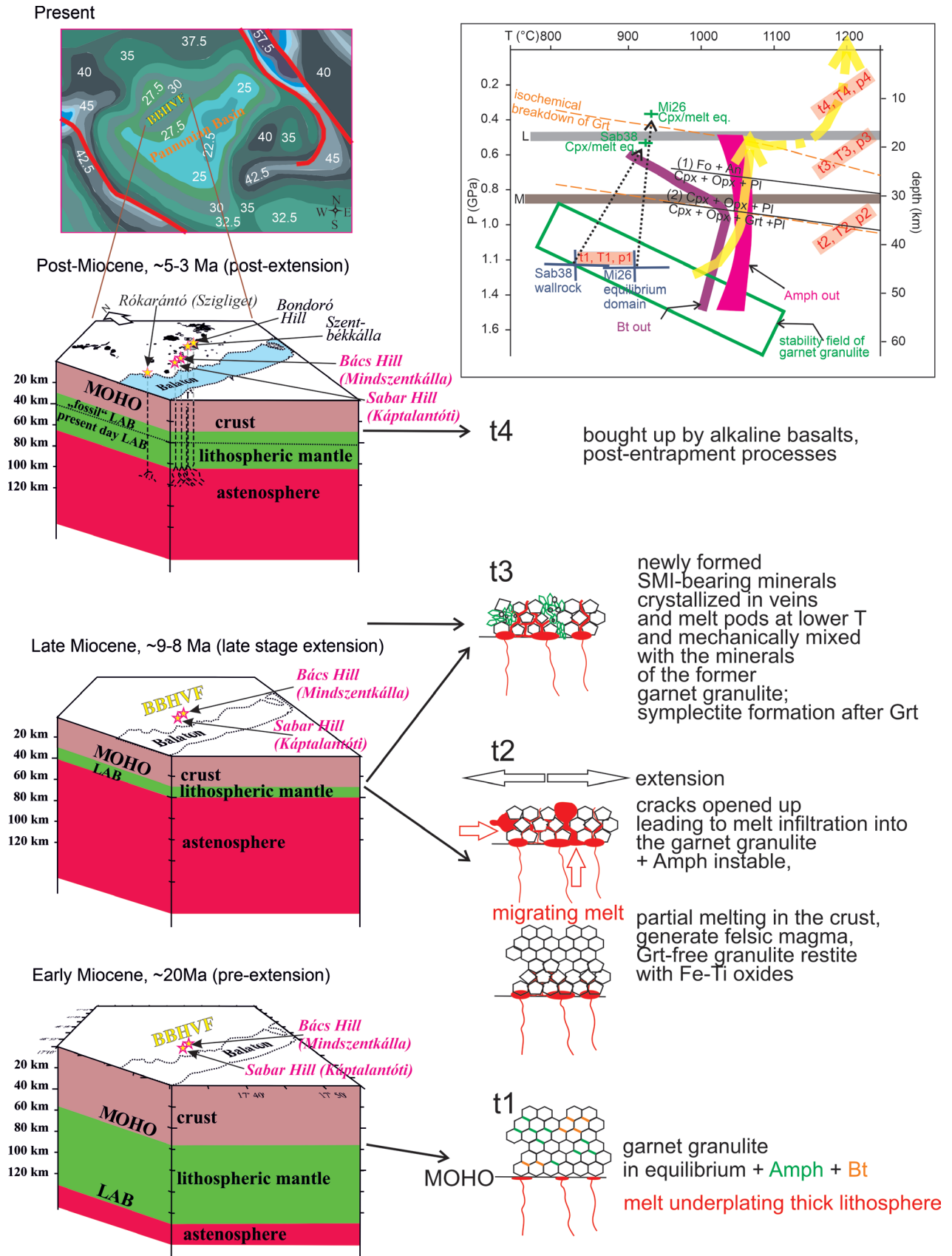
This early Miocene pre-extension equilibrium stage was followed by an extension (crustal thinning), which resulted in uplift of the lower crustal material. This process was accompanied by decompression melting during the Miocene. This partial melting in the lower crust generated felsic magmas and garnet-free granulite restites with Fe–Ti oxides. During the extension, cracks opened up and provided pathways to the migrating melt (Fig. 9 – t2 step). On the basis of the textural evidence, lower crust domains represented by xenoliths Mi26 and Sab38

were already out of the garnet stability field when partial melting affected their lithology (Fig. 9). Non-equilibrium microtexture and atoll-shape symplectites after the garnet show that these reactions were active in the final stages of crustal exhumation when the decreasing pressure induced the breakdown of garnets (early late Miocene, Németh et al. 2015).

Following partial melting, the original garnet granulitic mineral assemblage (garnet–clinopyroxene–plagioclase–titanite) was overprinted by newly formed, primary SMI-bearing plagioclase, clinopyroxene, and ilmenite mineral assemblages in veins (Sab38) and pods (Mi26) (Fig. 9 – t3 step). This newly formed mineral association was garnet-free (Figs. 2c, d, 8a and b) indicating that the crystallization occurred out of the stability field of the garnet (Fig. 9) sometime after the Miocene. Clinopyroxene-melt barometry confirms the pressure decrease (3.7 and 5.6 kbar for the Mi26 and Sab38 granulites) compared to the equilibrium stage of the garnet granulite (12 kbar, Németh et al. 2015). Moreover, this is in agreement with the geophysical data of the present-day thickness of the lower (18–20 km) and upper crust (10–12 km) (Mituch & Posgay 1972; Posgay et al. 1991, Horváth et al. 2015). The maximum depth of the lower crust is inferred from the garnet breakdown, which could have occurred shallower than about 30 km (Török et al. 2005; Dégi et al. 2010). This roughly corresponds to the base of the present-day crust where the stable mineral assemblage of the mafic granulites is clinopyroxene–orthopyroxene–plagioclase (Török 2012). The lower crust then extended upwards towards shallower depth, into the stability field of the olivine–plagioclase assemblage (Fig. 9). Thus, the melt-rock reactions took place at depths similar to the present-day lower crust with the final recrystallized garnet-free clinopyroxene–plagioclase pockets and veins. This means that silicate melt/rock interactions may have happened during the latest stage of crustal thinning or just after it in the early late Miocene (ca. 8–9 Ma; Fig. 9 – t3 step) when garnet was not stable.

We calculated equilibrium T conditions around 930 °C for the SMIs and their host clinopyroxene on the basis of Putirka (2008). This overlaps with the results of equilibrium T calculated between plagioclase and melt (860–890 °C). This temperature range is close to the maximum of the calculated equilibrium temperature of the granulite itself (850–930 °C in Németh et al. 2015). This suggests that the crystallization of the newly formed plagioclase and clinopyroxene in the leucosomes happened at the same temperature as the equilibrium temperature of the granulitic melanosome part.

The calculated temperature between plagioclase and melt depends on the H_2O content of the melt, which was around 4.5 wt. % in the Mi26 granulite and 3.3 wt. % in Sab38 granulite, respectively (Suppl. Table S3). These values have been calculated with the plagioclase-melt hygrometer of Putirka (2008) and were verified by the thermometer (Putirka 2008). Similar values can be obtained by the method of Devine et al. (1995) (Suppl. Table S2). These values are in good agreement with Németh et al. (2015), who showed that the melt re-hydrated the originally dry garnet granulite minerals with ~400 ppm

Present

Post-Miocene, ~5-3 Ma (post-extension)

t4   bought up by alkaline basalts,
       post-entrapment processes

t3   newly formed
       SMI-bearing minerals
       crystallized in veins
       and melt pods at lower T
       and mechanically mixed
       with the minerals
       of the former
       garnet granulite;
       symplectite formation after Grt

Late Miocene, ~9-8 Ma (late stage extension)

t2   extension

       cracks opened up
       leading to melt infiltration into
       the garnet granulite
       + Amph instable,

migrating melt   partial melting in the crust,
                   generate felsic magma,
                   Grt-free granulite restite
                   with Fe-Ti oxides

Early Miocene, ~20Ma (pre-extension)

t1   garnet granulite
       in equilibrium + Amph + Bt

MOHO   melt underplating thick lithosphere

⭐ **Localities of lower crustal garnet granulite xenoliths**
Áldozótető (Bondoró Hill), Szentbékkálla, Rókarántó (Szigliget),
Bács Hill (Mindszentkálla), Sabar Hill (Káptalantóti)

Fig. 9. Evolution of the crustal domain represented by the garnet granulite xenoliths. The upper right map is the present-day crustal thickness map of the Pannonian Basin from Fig. 1. Below that, three block diagrams show the evolution of the lithosphere under the Bakony–Balaton Highland Volcanic Field (BBHVF). On the right, the cartoons show the reconstructed evolution of the fluid-rock interaction history from t1 to t5. On the upper right there is a summary p–T–depth diagram with the known development history of the garnet granulite lower crust, based on xenoliths. Abbreviations: p – pressure; T – temperature; t – time; M – the present-day MOHO (Posgay et al. 1991); L – the present-day lower crust (Mituch & Posgay 1972; Szafián et al. 1999, Horváth et al. 2015); LAB – Lithosphere–Asthenosphere Boundary. The abbreviation of the minerals follows Kretz (1983). The green box marks the equilibrium pressure and temperature range of the mafic garnet granulites from the BBHVF based on Török et al. (2005). The blue and green crosses mark the equilibrium p–T ranges of the melanosome part of the studied granulite xenoliths and of the leucosome part of the xenoliths based on clinopyroxene-melt equilibria (Putirka et al. 2003; Putirka 2008). The dotted black arrows show the p–T path of the studied granulite xenoliths. The two orange dashed lines delineate the pressure range of the observed breakdown reaction of garnets (Dégi et al. 2010; Török 2012). The yellow continuous and dashed arrows indicate the evolutionary pathway based on garnet granulite xenoliths and the uplift of the xenoliths by the alkaline basalt in general from the BBHVF. The t–p–T labels show the melt-rock interaction steps at a given point in time, pressure, and temperature. In addition to felsic lithology, the appearance of the garnet is marked by the orange dashed line at the top (Vielzeuf & Schmidt 2001). Reaction (1) indicates the stability of the forsterite+anorthite mineral assemblage (Kushiro & Yoder 1966), whereas Reaction (2) marks the lower equilibrium limit of the garnet in addition to mafic lithology (Irving 1974). The Bt-out and Am-out curves are after Nair & Chacko (2002), and Springer & Seck (1997), respectively.

"H_2O"-content in the leucosome part of the xenoliths compared to <100 ppm "H_2O"-content in the melanosome.

Cenozoic crustal evolution beneath the BBHVF

Based on radiogenic and oxygen isotopic studies of garnet granulites, Dobosi et al. (2003) concluded that a part of the mafic lower crust beneath the BBHVF is the result of metamorphism of variously altered oceanic crust. The composition of the SMIs in our study also suggests the presence of MORB-derived rocks in the lower crust. However, the substantial contribution of a metasedimentary source is also required to explain its chemical composition. The MORB composition of the metabasalt component refers to a subduction-related origin. The age of such subduction is unconstrained but could have happened during the protracted contraction of the Alpine–Carpathian–Dinaridic orogen (Schmid et al. 2008, 2020).

On the other hand, the major and trace element composition of the SMIs show similarities to that of the middle Miocene calc-alkaline magmas (e.g., Harangi et al. 2001, Figs. 3, 4, 8a and c), which are widely present in the CPR (Fig. 1a). Based on geochemical evidence, Harangi et al. (2001) suggested that mixing of lower crustal metasediments with mantle-derived magma was responsible for the generation of the calc-alkaline rocks in the CPR. They calculated mixing between these two suspected end members and suggested 20–25 % to 40–50 % lower-crustal component in the andesites to rhyodacites. Such a large amount of assimilation requires a high heat flow beneath the PB, which could be connected to the upwelling of hot asthenosphere associated with the extensional thinning of the lithosphere and the intrusion of mantle-derived magmas (e.g., Szabó et al. 1992; Falus et al. 2000; Harangi 2001; Šumanovac 2015). Present-day heat flow ranges between 80–120 mW/m^2 but thermal modelling, and modern numerical modelling demonstrate higher values at the end of the rifting process (Dövényi & Horváth 1988; Lenkey et al. 2002; Balázs et al. 2017).

It is possible that the origin of the calc-alkaline rocks in the region is connected to a melt, formed by the same mechanism as suggested for the SMIs in the studied granulite xeno-

liths. Partial melting of a lower crustal MORB-like metamafic rock mixed with metasediments could occur in an extensional geodynamic setting at least in Börzsöny and Visegrád Mts. (Harangi et al. 2001). The melt inclusions themselves and the clinopyroxene–plagioclase veins and pockets are witnesses to such a process. Here we demonstrate that this melting beneath the BBHVF could have occurred during the late stage of crustal thinning, close to a situation with the present-day crustal thickness. However, according to the present state of knowledge on the evolution of the lithosphere in the Pannonian Basin, partial melting of the mafic granulite occurred during several stages (Török 2012). Furthermore, relics of hydrous minerals included in newly formed anhydrous reaction products (Fig. 2a) show evidence of dehydration melting/metasomatism at different depths in the lower crust (Fig. 9). Some (garnet–clinopyroxene–orthopyroxene–plagioclase, Sabar Hill) xenoliths indicate that garnets formed during these processes (quartz and apatite inclusions in garnet, Fig. 2b), i.e., melting took place at relatively high pressure, probably at the beginning of crustal thinning. In other xenoliths, magmatic microtexture was observed at a pressure lower than the stability field of garnet (Török 2012), which is also visible in the two studied xenoliths. The newly formed clinopyroxene–plagioclase domains consumed the symplectites formed after garnets (Fig. 2), which suggests that the extension had already started by the time when the metasomatizing melt infiltrated/percolated the crust (Fig. 9). Considering the previously described petrographic evidence from the granulite xenoliths from BBHVF, one might assume that partial melting primarily happened in the lower crust, where garnet–clinopyroxene–plagioclase restite (garnet granulites) remained. Thus, peritectic garnet could have crystallized at this depth (Fig. 2b). Following garnet crystallization, a fractionated melt migrated in the crust and formed the Pl-rich veins and pockets (Fig. 2) with a composition similar to the garnet-free Cpx–Pl granulites with magmatic microtexture (Török 2012). This option is supported by the presence of the garnet in every metapelitic granulite and in most metabasic granulites from the BBHVF (e.g., Török 1995; Dégi & Török 2003; Dégi et al. 2009, 2010; Downes et al. 2015).

On the other hand, some petrographic features and geochemical characteristics cannot be explained based on the present

data set. If garnet had crystallized from the melt even in a peritectic reaction or during fractional crystallization, the HREE concentration of generated melt would have decreased to a greater extent than we observed in Fig. 8a. As we stated, earlier composition of the melt trapped in Cpx, considered to be the closest one to the initial melt composition, shows high Yb content with a low Ce/Yb ratio. This feature suggests that garnet was not in equilibrium with the generated melt and could not have crystallized earlier (Fig. 8a). At the same time a melt related to the partial melting of a plagioclase+clinopyroxene+ orthopyroxene+ilmenite residual assemblage might have been originated with a similar trace element signal (Fig. 8b). However, this model requires further natural examples since granulites with this mineral association have not yet been found.

Numerical model of Annen et al. (2005) suggests that continuous emplacement of hydrous basaltic magma into different depths of the lower crust can generate a deep crustal hot zone. Numerical modelling of this hot zone shows that melts are generated from two distinct sources: partial crystallization of basaltic sills to produce residual H_2O-rich melts, and partial melting of pre-existing crustal rocks. Geophysical measurements can only detect sills beyond a certain thickness, and the deeper the sills are searched, the worse the resolution, so their presence in the lower crust below the BBHVF is questionable (e.g., Kiss et al. 2017). However, the geomagnetic studies suggest that most magnetic anomalies fit the location of the alkaline basaltic hills, not all anomalies are related to their necks/vents alone (Bence et al. 1988). Basalts trapped in Pannonian sediments have also been found (Bihari et al 1987). The geophysical studies, therefore, confirm the presence of basaltic dykes and sills in shallow crustal depths, which suggests that sills can be possibly present in the deep crust.

The continuous supply of the fresh mafic melt provides enough heat and volatiles for partially melting the surrounding lower crust and generating hybrid magmas, and the melting can affect metasedimentary and metaigneous basement rocks as we have shown in this study. Although this model is contributed to the magma generation in a case of as thickened crust, its effectiveness is questionable in this scenario. As the late-stage of extension occurred during the late middle to early late Miocene in the Pannonian Basin (Fig. 9) it might have helped magma ascent but at the same time suppressed the development of lower crustal hot zones to some extent. Although the granulites under the BBHVF were generally dry, SMIs rich in fluid-mobile elements partly re-hydrated the dry garnet granulite (Németh et al. 2015).

Conclusions

• The non-equilibrium microtextural domains, the clinopyroxene–ilmenite±plagioclase intergrowth and the existence of the plagioclase-enriched SMI-bearing vein and pockets in garnet granulite xenoliths suggest an interaction between the mafic granulite wall-rock and a percolating felsic silicate melt.

• The major and trace element composition of the SMIs suggests that the ones trapped in clinopyroxene are the closest to the original metasomatic melt, which is derived by the melting of a metasediment-(MORB) metabasalt (formerly amphibolite) mélange.

• The plagioclase and ilmenite hosted SMIs represent melt droplets remaining after various degrees of melt-garnet granulite interaction. The reaction that formed clinopyroxene–ilmenite±plagioclase symplectites required pre-existing titanite whose reaction with the felsic silicate melt to produce the mineral assemblage and a modified silicate melt, which can now be traced in the SMIs in the ilmenite.

• Continuous process of crustal thinning most probably linked with the extension of the Pannonian Basin. During progressive steps of the extension, melting of the granulitic lower crust registered in the studied garnet granulite xenoliths, at least partly during the late stage of this process, probably at the early late Miocene.

• SMIs are similar in composition to the middle Miocene calc-alkaline magmas from the northern Pannonian Basin. Thus, we suggest that a peraluminous silicic crustal melt find in the SMIs formed by a similar mechanism, as described here, might have contributed to the formation of CPR calc-alkaline rocks.

References

Annen C., Blundy J.D. & Sparks R.S.J. 2005: The Genesis of Intermediate and Silicic Magmas in Deep Crustal Hot Zones. *Journal of Petrology* 47, 505–539. https://doi.org/10.1093/petrology/egi084

Aranovich L.Y. 2017: The role of brines in high-temperature metamorphism and granitization. *Petrology* 25, 486–497. https://doi.org/10.1134/S0869591117050022

Balázs A., Matenco L., Magyar I., Horváth F. & Cloetingh S. 2016: The link between tectonics and sedimentation in back-arc basins: New genetic constraints from the analysis of the Pannonian Basin. *Tectonics* 35, 1526–1559. https://doi.org/10.1002/2015TC004109

Balázs A., Burov E., Matenco L., Vogt K., Francois T. & Cloetingh S. 2017: Symmetry during the syn- and post-rift evolution of extensional back-arc basins: The role of inherited orogenic structures. *Earth and Planetary Science Letters* 462, 86–98. https://doi.org/10.1016/j.epsl.2017.01.015

Bali E., Falus Gy., Szabó Cs., Peate D.W., Hidas K., Török K. & Ntaflos T. 2007: Remnants of boninitic melts in the upper mantle beneath the central Pannonian Basin? *Mineralogy and Petrology* 90, 51–72. https://doi.org/10.1007/s00710-006-0167-z

Balogh K., Vass D. & Ravasz-Baranyai L. 1994: K/Ar ages in the case of correlated K and excess Ar concentrations: A case study for

the alkaline olivine basalt of Somoska, Slovak–Hungarian frontier. *Geologica Carpathica* 45, 97–102.

Barich A., Acosta-Vigil A., Garrido C.J., Cesare B., Tajčmanová L. & Bartoli O. 2014: Microstructures and petrology of melt inclusions in the anatectic sequence of Jubrique (Betic Cordillera, S Spain): Implications for crustal anatexis. *Lithos* 206–207, 303–320. https://doi.org/10.1016/j.lithos.2014.08.003

Bartoli O. & Cesare B. 2020: Nanorocks: a 10-year-old story. *Rendiconti Lincei-Scienze Fisiche e Naturali* 31, 249–257. https://doi.org/10.1007/s12210-020-00898-7

Bartoli O., Acosta-Vigil A., Tajčmanová L., Cesare B. & Bodnar R.J. 2016: Using nanogranitoids and phase equilibria modeling to unravel anatexis in the crustal footwall of the Ronda peridotites (Betic Cordillera, S Spain). *Lithos* 256, 282–299. https://doi.org/10.1016/j.lithos.2016.03.016

Bence G., Bihari D. & Lantos M. 1988: Geomagnetic detection of basaltic volcanic vents on the Balaton Highland [Bazaltvulkáni kürtők kimutatása mágneses módszerrel a Balaton-felvidéken]. Annual Report of the Geological Institute of Hungary from 1988, 363–369 (in Hungarian). http://epa.oszk.hu/02900/02934/00017/pdf/EPA02934_mafi_evi_jelentes_1988-I_363-369.pdf

Bihari D., Csathó B., Csillag G., Hoffer E. & Schőnviszky L. 1987: Geophysical exploration of the Balaton Highland [A Balaton-felvidék geofizikai kutatása]. Annual Report of the Eötvös Loránd Geophysical Institute of Hungary from 1986, 26–27 (in Hungarian). https://epa.oszk.hu/03100/03104/00024/pdf/EPA03104_elgi_jelentes_1986_011-027.pdf

Bodnar R.J. & Frezzotti M.-L. 2020: Microscale Chemistry: Raman Analysis of Fluid and Melt Inclusions. *Elements: An International Magazine of Mineralogy, Geochemistry, and Petrology* 16, 93–98.

Borghini A., Ferrero S., Wunder B., Laurent O., O'Brien P.J. & Ziemann M.A. 2018: Granitoid melt inclusions in orogenic peridotite and the origin of garnet clinopyroxenite. *Geology* 46, 1007–1010. https://doi.org/10.1130/G45316.1

Borghini A., Ferrero S., O'Brien P.J., Laurent O., Günter C. & Ziemann M.A. 2020: Cryptic metasomatic agent measured in situ in Variscan mantle rocks: Melt inclusions in garnet of eclogite, Granulitgebirge, Germany. *Journal of Metamorphic Geology* 38, 207–234. https://doi.org/10.1111/jmg.12519

Carvalho B.B., Bartoli O., Cesare B., Tacchetto T., Gianola O., Ferri F. & Szabó Cs. 2020: Primary CO_2-bearing fluid inclusions in granulitic garnet usually do not survive. *Earth and Planetary Science Letters* 536, 116170. https://doi.org/10.1111/jmg.12463

Castro A., Patiño Douce A.E., Corretgé L.G., de la Rosa J.D., El-Biad M. & El-Hmidi H. 1999: Origin of peraluminous granites and granodiorites, Iberian Massif, Spain: an experimental test of granite petrogenesis. *Contributions to Mineralogy and Petrology* 135, 255–276. https://doi.org/10.1007/s004100050511

Castro A., Gerya T., García-Casco A., Fernández C., Díaz-Alvarado J., Moreno-Ventas I. & Löw I. 2010: Melting Relations of MORB–Sediment Mélanges in Underplated Mantle Wedge Plumes; Implications for the Origin of Cordilleran-type Batholiths. *Journal of Petrology* 51, 1267–1295. https://doi.org/10.1093/petrology/egq019

Cesare B., Maineri C., Toaldo A.B., Pedron D. & Vigil A.A. 2007: Immiscibility between carbonic fluids and granitic melts during crustal anatexis: a fluid and melt inclusion study in the enclaves of the Neogene Volcanic Province of SE Spain. *Chemical Geology* 237, 433–449. https://doi.org/10.1016/j.chemgeo.2006.07.013

Cesare B., Ferrero S., Salvioli-Mariani E., Pedron, D. & Cavallo A. 2009: "Nanogranite" and glassy inclusions: The anatectic melt in migmatites and granulites. *Geology* 37, 627–630. https://doi.org/10.1130/G25759A.1

Cesare B., Acosta-Vigil A., Ferrero S. & Bartoli O. 2011: Melt inclusions in migmatites and granulites. *Journal of the Virtual Explorer* 38, 1441–8142.

Cesare B., Acosta-Vigil A., Bartoli O. & Ferrero S. 2015: What can we learn from melt inclusions in migmatites and granulites? *Lithos* 239, 186–216. https://doi.org/10.1016/j.lithos.2015.09.028

Clemens J.D. 1990: The Granulite–Granite Connexion. In: Vielzeuf D. & Vidal P. (Eds.): Granulites and Crustal Evolution. NATO ASI Series (Series C: Mathematical and Physical Sciences), vol. 311. *Springer*, Dordrecht, 25–36. https://doi.org/10.1007/978-94-009-2055-2_3

Créon L., Rouchon V., Youssef S., Rosenberg E., Delpech G., Szabó Cs., Remusat L., Mostefaoui S., Asimow P.D. & Antoshechkina P.M. 2017: Highly CO_2-supersaturated melts in the Pannonian lithospheric mantle – A transient carbon reservoir? *Lithos* 286, 519–533. https://doi.org/10.1016/j.lithos.2016.12.009

Csontos L. & Vörös A. 2004: Mesozoic plate tectonic reconstruction of the Carpathian region. *Palaeogeography, Palaeoclimatology, Palaeoecology* 210, 1–56. https://doi.org/https://doi.org/10.1016/j.palaeo.2004.02.033

Csontos L., Nagymarosy A., Horváth F. & Kováč M. 1992: Tertiary evolution of the Intra-Carpathian area: a model. *Tectonophysics* 208, 221–241. https://doi.org/10.1016/0040-1951(92)90346-8

Dégi J. & Török K. 2003: Petrographic evidence of crustal thinning in Bakony-Balaton Highland Volcanic Field. *Magyar Geofizika* 44, 125–133 (in Hungarian).

Dégi J., Abart R., Török K., Rhede D. & Petrishcheva E. 2009: Evidence for xenolith–host basalt interaction from chemical patterns in Fe–Ti-oxides from mafic granulite xenoliths of the Bakony–Balaton Volcanic field (W-Hungary). *Mineralogy and Petrology* 95, 219–234. https://doi.org/10.1007/s00710-008-0035-0

Dégi J., Abart R., Török K., Bali E., Wirth R. & Rhede D. 2010: Symplectite formation during decompression induced garnet breakdown in lower crustal mafic granulite xenoliths: mechanisms and rates. *Contributions to Mineralogy and Petrology* 159, 293–314. https://doi.org/10.1007/s00410-009-0428-z

Devine J.D., Gardner J.E., Brack H.P., Layne G.D. & Rutherford M.J. 1995: Comparison of microanalytical methods for estimating H_2O contents of silicic volcanic glasses. *American Mineralogist* 80, 319–328. https://doi.org/10.2138/am-1995-3-413

Dobosi G., Kempton P.D., Downes H., Embey-Isztin A., Thirlwall M. & Greenwood P. 2003: Lower crustal granulite xenoliths from the Pannonian Basin, Hungary, Part 2: Sr–Nd–Pb–Hf and O isotope evidence for formation of continental lower crust by tectonic emplacement of oceanic crust. *Contributions to Mineralogy and Petrology* 144, 671–683. https://doi.org/10.1007/s00410-002-0422-1

Dövényi P. & Horváth F. 1988: A review of temperature, thermal conductivity,and heat flow data from the Pannonian basin, In: Royden L.H. & Horváth F. (Eds.): The Pannonian Basin: a study in basin evolution. *AAPG Memoir* 45, 195–235.

Downes H., Carter A., Armstrong R., Dobosi G. & Embey-Isztin A. 2015: Lower crustal zircons reveal Neogene metamorphism beneath the Pannonian Basin (Hungary). *Open Geoscience* 7, 223–233. https://doi.org/10.1515/geo-2015-0028

Embey-Isztin A., Dobosi G., Downes H., Poultidis C. & Scharbert H.G. 1993: A compilation of new major trace element and isotope geochemical analyses of the young alkali basalts from the Pannonian Basin. *Fragmenta Minerologica et Palaeontologica* 16, 5–26.

Embey-Isztin A., Downes H., Kempton P.D., Dobosi, G. & Thirlwall M. 2003: Lower crustal granulite xenoliths from the Pannonian Basin, Hungary. Part 1: mineral chemistry, thermobarometry and petrology. *Contributions to Mineralogy and Petrology* 144, 652–670. https://doi.org/10.1007/s00410-002-0421-2

Ewing T.A., Rubatto D. & Hermann J. 2014: Hafnium isotopes and Zr/Hf of rutile and zircon from lower crustal metapelites (Ivrea–

Verbano Zone, Italy): Implications for chemical differentiation of the crust. *Earth and Planetary Science Letters* 389, 106–118. https://doi.org/https://doi.org/10.1016/j.epsl.2013.12.029

Falus Gy., Szabó Cs. & Vaselli O. 2000: Mantle upwelling within the Pannonian Basin: evidence from xenolith lithology and mineral chemistry. *Terra Nova* 12, 295–302. https://doi.org/10.1046/j.1365-3121.2000.00313.x

Ferrero S., Bodnar R.J., Cesare B. & Viti C. 2011: Re-equilibration of primary fluid inclusions in peritectic garnet from metapelitic enclaves, El Hoyazo, Spain. *Lithos* 124, 117–131. https://doi.org/10.1016/j.lithos.2010.09.004

Ferrero S., Bartoli O., Cesare B., Salvioli-Mariani E., Acosta-Vigil A., Cavallo A., Groppo C. & Battiston S. 2012: Microstructures of melt inclusions in anatectic metasedimentary rocks. *Journal of Metamorphic Geology* 30, 303–322. https://doi.org/10.1111/j.1525-1314.2011.00968.x

Ferrero S., Wunder B., Walczak K., O'Brien P.J. & Ziemann M.A. 2015: Preserved near ultrahigh-pressure melt from continental crust subducted to mantle depths. *Geology* 43, 447–450. https://doi.org/10.1130/G36534.1

Ferrero S., Wunder B., Ziemann M.A., Wälle M. & O'Brien, P.J. 2016: Carbonatitic and granitic melts produced under conditions of primary immiscibility during anatexis in the lower crust. *Earth and Planetary Science Letters* 454, 121–131. https://doi.org/10.1016/j.epsl.2016.08.043

Ferrero S., Godard G., Palmeri R., Wunder B. & Cesare B. 2018a: Partial melting of ultramafic granulites from Dronning Maud Land, Antarctica: constraints from melt inclusions and thermodynamic modeling. *American Mineralogist* 103, 610–622. https://doi.org/10.2138/am-2018-6214

Ferrero S., O'Brien P.J., Borghini A., Wunder B., Wälle M., Günter C. & Ziemann M.A. 2018b: A treasure chest full of nanogranitoids: an archive to investigate crustal melting in the Bohemian Massif. *Geological Society London Special Publications* 478, 13–38. https://doi.org/10.1144/SP478.19

Ferri F. Cesare B., Bartoli O., Ferrero S., Palmeri R., Remusat L. & Poli S. 2020: Melt inclusions at MT. Edixon (Antarctica): Chemistry, petrology and implications for the evolution of the Lanterman range. *Lithos* 374, 105685. https://doi.org/10.1016/j.lithos.2020.105685

Fodor L., Csontos L., Bada G., Györfi I. & Benkovics L. 1999: Tertiary tectonic evolution of the Pannonian Basin system and neighbouring orogens: a new synthesis of palaeostress data. *Geological Society*, London, *Special Publications* 156, 295–334. https://doi.org/10.1144/GSL.SP.1999.156.01.15

Fodor L., Balázs A., Csillag G., Dunkl I., Héja G., Jelen B., Kelemen P., Kövér Sz., Németh A., Nyíri D., Selmeczi I., Trajanova M., Vrabec M. & Vrabec M. 2021: Crustal exhumation and depocenter migration from the Alpine orogenic margin towards the Pannonian extensional back-arc basin controlled by inheritance. *Global and Planetary Change* 201, 103475. https://doi.org/10.1016/j.gloplacha.2021.103475

Frezzotti M.-L. 2001: Silicate-melt inclusions in magmatic rocks: applications to petrology. *Lithos* 55, 273–299. https://doi.org/10.1016/S0024-4937(00)00048-7

Gaetani G.A. 2004: The influence of melt structure on trace element partitioning near the peridotite solidus. *Contributions to Mineralogy and Petrology* 147, 511–527. https://doi.org/10.1007/s00410-004-0575-1

Gianola O., Bartoli O., Ferri F., Galli A., Ferrero S., Capizzi L.S. & Cesare B. 2020: Anatectic melt inclusions in ultra high temperature granulites. *Journal of Metamorphic Geology* 39, 321–342. https://doi.org/10.1111/jmg.12567

Guillong M., Meier D., Allan M., Heinrich C.A. & Yardley B.W.D. 2008: SILLS: A MATLAB-based program for the reduction of laser ablation ICP-MS data of homogeneous materials and inclu-
sions. In: Sylvester P. (Ed.): Laser Ablation ICP-MS in the Earth Sciences: Current Practices and Outstanding Issues. *Mineralogical Association of Canada Short Course Series* 40, 328–333.

Hacker B.R. 1990: Amphibolite-facies-to-granulite-facies reactions in experimentally deformed, unpowdered amphibolite. *American Mineralogist* 75, 1349–1361.

Halter W.E., Pettke T., Heinrich C.A. & Rothen-Rutishauser B. 2002: Major to trace element analysis of melt inclusions by laser-ablation ICP-MS: methods of quantification. *Chemical Geology* 183, 63–86. https://doi.org/10.1016/S0009-2541(01)00372-2

Halter W.E., Pettke T. & Heinrich C.A. 2004: Laser-ablation ICP-MS analysis of silicate and sulfide melt inclusions in an andesitic complex I: analytical approach and data evaluation. *Contributions to Mineralogy and Petrology* 147, 385–396. https://doi.org/10.1007/s00410-004-0562-6

Harangi Sz. 2001: Neogene to Quaternary volcanism of the Carpathian–Pannonian Region – a review. *Acta Geologica Hungarica* 44, 223–258.

Harangi Sz. & Lenkey L. 2007: Genesis of the Neogene to Quaternary volcanism in the Carpathian-Pannonian region: role of subduction, extension, and mantle plume. *Special Papers*, *Geological Society of America* 418, 67–92.

Harangi Sz., Downes H., Kósa L., Szabó Cs., Thirlwall M., Mason P.R.D. & Mattey D. 2001: Almandine garnet in calc-alkaline volcanic rocks of the Northern Pannonian Basin (Eastern–Central Europe): Geochemistry, petrogenesis and geodynamic implications. *Journal of Petrology* 42, 1813–1843. https://doi.org/10.1093/petrology/42.10.1813

Heinrich C.A., Pettke T., Halter W.E., Aigner-Torres M., Audétat A., Günther D., Hattendorf B., Bleiner D., Guillong M. & Horn I. 2003: Quantitative multi-element analysis of minerals, fluid and melt inclusions by laser-ablation inductively-coupled-plasma mass-spectrometry. *Geochimica et Cosmochimica Acta* 67, 3473–3497. https://doi.org/10.1016/S0016-7037(03)00084-X

Hidas K., Guzmics T., Szabó Cs., Kovács I.J., Bodnar R.J., Zajacz Z., Nédli Z., Vaccari L. & Perucchi A. 2010: Coexisting silicate melt inclusions and H_2O-bearing, CO_2-rich fluid inclusions in mantle peridotite xenoliths from the Carpathian–Pannonian region (central Hungary). *Chemical Geology* 274, 1–18. https://doi.org/10.1016/j.chemgeo.2010.03.004

Hiroi Y., Hokada T., Kato M., Yanagi A., Adachi T., Osanai Y., Motoyoshi Y. & Shiraishi K. 2019: Felsite–nanogranite inclusions and three Al_2SiO_5 polymorphs in the same garnet in ultrahigh-temperature granulites from Rundvågshetta, Lützow–Holm Complex, East Antarctica. *Journal of Mineralogical and Petrological Sciences* 181118. https://doi.org/10.2465/jmps.181118

Hiroi Y., Hokada T., Kayama M., Miyake A., Adachi T., Prame B., Perera K., Satish-Kumar M., Osanai Y. & Motoyoshi Y. 2020: Zoned quartz phenocrysts in supercooled melt inclusions in granulites from continental collision orogens. *Island Arc* 29, e12374. https://doi.org/10.1111/iar.12374

Horváth F. 1993: Towards a mechanical model for the formation of the Pannonian basin. *Tectonophysics* 226, 333–357. https://doi.org/10.1016/0040-1951(93)90126-5

Horváth F., Musitz B., Balázs A., Végh A., Uhrin A., Nádor A., Koroknai B., Pap N., Tóth T. & Wórum G. 2015: Evolution of the Pannonian basin and its geothermal resources. *Geothermics* 53, 328–352. https://doi.org/10.1016/j.geothermics.2014.07.009

Huang F., Lundstrom C.C. & McDonough W.F. 2006: Effect of melt structure on trace-element partitioning between clinopyroxene and silicic, alkaline, aluminous melts. *American Mineralogist* 91, 1385–1400. https://doi.org/10.2138/am.2006.1909

Irving A.J. 1974: Geochemical and high pressure experimental studies of garnet pyroxenite and pyroxene granulite xenoliths from the Delegate basaltic pipes, Australia. *Journal of Petrology* 15, 1–40. https://doi.org/10.1093/petrology/15.1.1

Jugovics L. 1968: Structure of the basalt regions in the Balaton Highland. *Yearly Report of the Hungarian Geological Institute,* 75–82 (in Hungarian).

Kalmár D., Süle B., Bondár I. & the AlpArray Working Group 2018: Preliminary Moho depth determination from receiver function analysis using AlpArray stations in Hungary. *Acta Geodaetica et Geophysica* 53, 309–321. https://doi.org/10.1007/s40328-018-0218-z

Kázmér M. & Kovács S. 1985: Permian–Paleogene paleogeography along the eastern part of the Insubric-Periadriatic lineament system: evidence for continental escape of the Bakony-Drauzug unit. *Acta Geologica Hungarica* 28, 71–84.

Kempton P.D., Downes H. & Embey-Isztin A. 1997: Mafic granulite xenoliths in Neogene alkali basalts from the western Pannonian Basin: insights into the lower crust of a collapsed orogen. *Journal of Petrology* 38, 941–970. https://doi.org/10.1093/petroj/38.7.941

Kiss J., Vértesy L. & Gulyás Á. 2017: Geomagnetic case studies from the Balaton Highland, the Danube-Tisza Basin and the Tokaj Mountains [Földmágneses esettanulmányok a Balatonfelvidékről, a Duna-Tisza közéről és a Tokaji-hegység területéről]. *Magyar Geofizika* 57, 126–151 (in Hungarian).

Kovács I.J. & Szabó Cs. 2008: Middle Miocene volcanism in the vicinity of the Middle Hungarian zone: evidence for an inherited enriched mantle source. *Journal of Geodynamics* 45, 1–17. https://doi.org/10.1016/j.jog.2007.06.002

Kretz R. 1983: Symbols for rock-forming minerals. *American Mineralogist* 68, 277–279.

Kushiro I. & Yoder Jr H.S. 1966: Anorthite–forsterite and anorthite–enstatite reactions and their bearing on the basalt–eclogite transformation. *Journal of Petrology* 7, 337–362. https://doi.org/10.1093/petrology/7.3.337

Lenkey L., Dövényi P., Horváth F. & Cloetingh S.A.P.L. 2002: Geothermics of the Pannonian basin and its bearing on the neotectonics. *EGU Stephan Mueller Special Publication Series* 3, 1–12.

Manning C.E. 2018: Fluids of the lower crust: deep is different. *Annual Review of Earth and Planetary Sciences* 46, 67–97. https://doi.org/10.1146/annurev-earth-060614-105224

Manning C.E. & Aranovich L.Y. 2014: Brines at high pressure and temperature: thermodynamic, petrologic and geochemical effects. *Precambrian Research* 253, 6–16. https://doi.org/10.1016/j.precamres.2014.06.025

Maţenco L. & Radivojević D. 2012: On the formation and evolution of the Pannonian Basin: Constraints derived from the structure of the junction area between the Carpathians and Dinarides. *Tectonics* 31. https://doi.org/10.1029/2012TC003206

Mituch E. & Posgay K. 1972: Hungary. The crustal structure of Central and South-Eastern Europe based on the results of explosion seismology. *Geophysical Transactions* 28, 118–129.

Montel J.-M. & Vielzeuf D. 1997: Partial melting of metagreywackes, Part II. Compositions of minerals and melts. *Contributions to Mineralogy and Petrology* 128, 176–196. https://doi.org/10.1007/s004100050302

Nair R. & Chacko T. 2002: Fluid-absent melting of high-grade semi-pelites: P–T constraints on orthopyroxene formation and implications for granulite genesis. *Journal of Petrology* 43, 2121–2142. https://doi.org/10.1093/petrology/43.11.2121

Németh B., Török K., Kovács I., Szabó Cs., Abart R., Dégi J., Mihály J. & Németh Cs. 2015: Melting, fluid migration and fluid-rock interactions in the lower crust beneath the Bakony–Balaton Highland volcanic field: a silicate melt and fluid inclusion study. *Mineralogy and Petrology* 109, 217–234. https://doi.org/10.1007/s00710-015-0366-6

Newton R.C., Aranovich L.Y., Hansen E.C. & Vandenheuvel B.A. 1998: Hypersaline fluids in Precambrian deep-crustal metamorphism. *Precambrian Research* 91, 41–63. https://doi.org/10.1016/S0301-9268(98)00038-2

Nicoli G. & Ferrero S. 2021: Nanorocks, volatiles and plate tectonics. *Geoscience Frontiers* 12, 101188. https://doi.org/10.1016/j.gsf.2021.101188

Patiño-Douce A.E. & Beard J.S. 1995: Dehydration-melting of biotite gneiss and quartz amphibolite from 3 to 15 kbar. *Journal of Petrology* 36, 707–738. https://doi.org/10.1093/petrology/36.3.707

Pearce J.A. 1983: Role of the sub-continental lithosphere in magma genesis at active continental margins. In: Hawkesworth C.J. & Norry M.J. (Eds.): Continental basalts and mantle xenoliths. *Shiva Publications*, Nantwich, Cheshire, 230–249.

Peterson J.W. & Newton R.C. 1990: Experimental biotite-quartz melting in the KMASH-CO$_2$ system and the role of CO$_2$ in the petrogenesis of granites and related rocks. *American Mineralogist* 75, 1029–1042.

Posgay K., Albu I., Mayerová M., Nakládalová Z., Ibrmajer I., Blizkovsky M., Aric K. & Gutdeutsch R. 1991: Contour Map of the Mohorovicic Discontinuity Beneath Central Europe. *Geophysical Transactions* 36, 7–13.

Putirka K.D. 2008: Thermometers and barometers for volcanic systems. *Reviews in mineralogy and geochemistry* 69, 61–120. https://doi.org/10.2138/rmg.2008.69.3

Putirka K.D., Ryerson F.J. & Mikaelian H. 2003: New igneous thermobarometers for mafic and evolved lava compositions, based on clinopyroxene+liquid equilibria. *American Mineralogist* 88, 1542–1554. https://doi.org/10.2138/am-2003-1017

Qian Q. & Hermann J. 2013: Partial melting of lower crust at 10–15 kbar: Constraints on adakite and TTG formation. *Contributions to Mineralogy and Petrology* 165, 1195–1224. https://doi.org/10.1007/s00410-013-0854-9

Rasmussen D.J., Plank T.A., Roman D.C., Power J.A., Bodnar R.J. & Hauri E.H. 2018: When does eruption run-up begin? Multidisciplinary insight from the 1999 eruption of Shishaldin volcano. *Earth and Planetary Science Letters* 486, 1–14. https://doi.org/10.1016/j.epsl.2018.01.001

Roedder E. 1992: Fluid inclusion evidence for immiscibility in magmatic differentiation. *Geochimica et Cosmochimica Acta* 56, 5–20. https://doi.org/10.1016/0016-7037(92)90113-W

Royden L.H. 1988: Late Cenozoic Tectonics of the Pannonian Basin System: Chapter 3. *AAPG Memoir* 45, 27–48.

Rudnick R.L. & Gao S. 2003: Composition of the continental crust. The crust 3. In: Holland H. D. & Turekian K. K. (Eds.): Treatise on Geochemistry. *Pergamon*, 1–64. https://doi.org/10.1016/B0-08-043751-6/03016-4

Safonov O.G., Mityaev A.S., Yapaskurt V.O., Belyanin G.A., Elburg M., Rajesh H.M. & Smit A.C. 2020: Carbonate-silicate inclusions in garnet as evidence for a carbonate-bearing source for fluids in leucocratic granitoids associated with granulites of the Southern Marginal Zone, Limpopo Complex. South Africa. *Gondwana Research* 77, 147–167. https://doi.org/10.1016/j.gr.2019.07.012

Saunders A.D., Norry M.J. & Tarney J. 1991: Fluid influence on the trace element compositions of subduction zone magmas. *Philosophical Transactions of the Royal Society of London. Series A: Physical and Engineering Sciences* 335, 377–392. https://doi.org/10.1098/rsta.1991.0053

Sawyer E.W. 1987: The role of partial melting and fractional crystallization in determining discordant migmatite leucosome compositions. *Journal of Petrology* 28, 445–473. https://doi.org/10.1093/petrology/28.3.445

Schmid S.M., Bernoulli D., Fügenschuh B., Matenco L., Schefer S., Schuster R., Tischler M. & Ustaszewski K. 2008: The Alpine–Carpathian–Dinaridic orogenic system: correlation and evolution of tectonic units. *Swiss Journal of Geosciences* 101, 139–183. https://doi.org/10.1007/s00015-008-1247-3

Schmid S.M., Fügenschuh B., Kounov A., Maţenco L., Nievergelt P., Oberhänsli R., Pleuger J., Schefer S., Schuster R. & Tomljenović B.

2020: Tectonic units of the Alpine collision zone between Eastern Alps and western Turkey. *Gondwana Research* 78, 308–374. https://doi.org/10.1016/j.gr.2019.07.005

Springer W. & Seck H.A. 1997: Partial fusion of basic granulites at 5 to 15 kbar: implications for the origin of TTG magmas. *Contributions to Mineralogy and Petrology* 127, 30–45. https://doi.org/10.1007/s004100050263

Steele-MacInnis M., Esposito R. & Bodnar R.J. 2011: Thermodynamic Model for the Effect of Post-entrapment Crystallization on the H_2O–CO_2 Systematics of Vapor-saturated, Silicate Melt Inclusions. *Journal of Petrology* 52, 2461–2482. https://doi.org/10.1093/petrology/egr052

Šumanovac F. 2015: Lithosphere model of the Pannonian–Adriatic overthrusting. *Tectonophysics* 665, 79–91. https://doi.org/10.1016/j.tecto.2015.09.032

Sun S.-S. & McDonough W.F. 1989: Chemical and isotopic systematics of oceanic basalts: implications for mantle composition and processes. *Geological Society, London, Special Publications* 42, 313–345.

Szabó Cs., Csontos L. & Harangi Sz. 1992: Review of Neogene and Quaternary volcanism of the Carpathian–Pannonian region. *Geodynamics of rifting* 1, 243–256. https://doi.org/10.1016/B978-0-444-89912-5.50018-1

Szafián P., Tari G., Horváth F. & Cloetingh S. 1999: Crustal structure of the Alpine–Pannonian transition zone: a combined seismic and gravity study. *International Journal of Earth Sciences* 88, 98–110. https://doi.org/10.1007/s005310050248

Tacchetto T., Bartoli O., Cesare B., Berkesi M., Aradi L.E., Dumond G. & Szabó Cs. 2019: Multiphase inclusions in peritectic garnet from granulites of the Athabasca granulite terrane (Canada): Evidence of carbon recycling during Neoarchean crustal melting. *Chemical Geology* 508, 197–209. https://doi.org/10.1016/j.chemgeo.2018.05.043

Török K. 1995: Garnet breakdown reaction and fluid inclusions in a garnet–clinopyroxenite xenolith from Szentbékkálla (Balaton-Highland, Western Hungary). *Acta Vulcanologica* 7, 285–290.

Török K. 2002: Ultrahigh-temperature metamorphism of a buchitized xenolith from the basaltic tuff of Szigliget (Hungary). *Acta Geologica Hungarica* 45, 175–192. https://doi.org/10.1007/s00531-011-0743-2

Török K. 2012: On the origin and fluid content of some rare crustal xenoliths and their bearing on the structure and evolution of the crust beneath the Bakony–Balaton Highland Volcanic Field (W-Hungary). *International Journal of Earth Sciences* 101, 1581–1597.

Török K., Bali E., Szabó Cs. & Szakál J.A. 2003: Sr-barite droplets associated with sulfide blebs in clinopyroxene megacrysts from basaltic tuff (Szentbékkálla, western Hungary). *Lithos* 66, 275–289. https://doi.org/10.1016/S0024-4937(02)00223-2

Török K., Dégi J., Szép A. & Marosi G. 2005: Reduced carbonic fluids in mafic granulite xenoliths from the Bakony–Balaton Highland Volcanic Field, W-Hungary. *Chemical Geology* 223, 93–108. https://doi.org/10.1016/j.chemgeo.2005.05.010

Török K., Németh B., Koller F., Dégi J., Badenszki E., Szabó Cs. & Mogessie A. 2014: Evolution of the middle crust beneath the western Pannonian Basin: a xenolith study. *Mineralogy and Petrology* 108, 33–47. https://doi.org/10.1007/s00710-013-0287-1

Touret J.L.R. 1985: Fluid regime in southern Norway: the record of fluid inclusions. In: Tobi A.C. & Touret J.L.R. (Eds.): The Deep Proterozoic Crust in the North Atlantic Provinces. *NATO ASI Series (Series C: Mathematical and Physical Sciences)* 158, 517–549. *Springer*, Dordrecht. https://doi.org/10.1007/978-94-009-5450-2_30

Touret J.L.R. & Huizenga J.M. 2020: Large-scale fluid transfer between mantle and crust during supercontinent amalgamation and disruption. *Russian Geology and Geophysics* 61, 527–542. https://doi.org/10.15372/RGG2019128

Van Orman J.A., Grove T.L. & Shimizu N. 2001: Rare earth element diffusion in diopside: influence of temperature, pressure, and ionic radius, and an elastic model for diffusion in silicates. *Contributions to Mineralogy and Petrology* 141, 687–703. https://doi.org/10.1007/s004100100269

Vielzeuf D. & Montel J.-M. 1994: Partial melting of metagreywackes. Part I. Fluid-absent experiments and phase relationships. *Contributions to Mineralogy and Petrology* 117, 375–393. https://doi.org/10.1007/BF00307272

Vielzeuf D. & Schmidt M.W. 2001: Melting relations in hydrous systems revisited: application to metapelites, metagreywackes and metabasalts. *Contributions to Mineralogy and Petrology* 141, 251–267. https://doi.org/10.1007/s004100100237

Weinberg R. F. & Hasalová P. 2015: Water-fluxed melting of the continental crust: A review. *Lithos* 212, 158–188. https://doi.org/10.1016/j.lithos.2014.08.021

Wijbrans J., Németh K., Martin U. & Balogh K. 2007: $^{40}Ar/^{39}Ar$ geochronology of Neogene phreatomagmatic volcanism in the western Pannonian Basin, Hungary. *Journal of Volcanology and Geothermal Research* 164, 193–204. https://doi.org/10.1016/j.jvolgeores.2007.05.009

Zajacz Z. & Halter W.E. 2007: LA-ICPMS analyses of silicate melt inclusions in co-precipitated minerals: Quantification, data analysis and mineral/melt partitioning. *Geochimica et Cosmochimica Acta* 71, 1021–1040. https://doi.org/https://doi.org/10.1016/j.gca.2006.11.001

Zajacz Z., Kovács I.J., Szabó Cs., Halter W.E. & Pettke T. 2007: Evolution of mafic alkaline melts crystallized in the uppermost lithospheric mantle: a melt inclusion study of olivine–clinopyroxenite xenoliths, northern Hungary. *Journal of Petrology* 48, 853–883. https://doi.org/10.1093/petrology/egm004

Electronic supplementary material is available online at:

Suppl. Fig. S1 at http://geologicacarpathica.com/data/files/supplements/GC-72-3-Nemeth_FigS1.jpg.
Suppl. Fig. S2 at http://geologicacarpathica.com/data/files/supplements/GC-72-3-Nemeth_FigS2.jpg.
Suppl. Table S1 at http://geologicacarpathica.com/data/files/supplements/GC-72-3-Nemeth_TableS1.xlsx.
Suppl. Table S2 at http://geologicacarpathica.com/data/files/supplements/GC-72-3-Nemeth_TableS2.xlsx.
Suppl. Table S3 at http://geologicacarpathica.com/data/files/supplements/GC-72-3-Nemeth_TableS3.xlsx.
Suppl. Table S4 at http://geologicacarpathica.com/data/files/supplements/GC-72-3-Nemeth_TableS4.xlsx.